UNCLASSIFIED

| AD NUMBER |
| --- |
| AD484821 |
| LIMITATION CHANGES |

TO:

Approved for public release; distribution is unlimited. Document partially illegible.

FROM:

Distribution authorized to U.S. Gov't. agencies and their contractors; Administrative/Operational Use; JUL 1966. Other requests shall be referred to Arnold Engineering Development Center, Arnold AFB, TN. Document partially illegible.

| AUTHORITY |
| --- |
| AEDC/IN STINFO, via memorandum dtd 29 Jan 1996 |

THIS PAGE IS UNCLASSIFIED

AEDC-TR-66-32

$A \& DC/PA 96 - 284$

AUG 10 1966

OCT 18 1966

SEP 3 1971

APR 1 3 1988

DEC 0 1 1995

# TURBULENT WAKE AND SHOCK SHAPE
# OF HYPERVELOCITY SPHERES

A. B. Bailey

ARO, Inc.

July 1966

# VON KÁRMÁN GAS DYNAMICS FACILITY
# ARNOLD ENGINEERING DEVELOPMENT CENTER
# AIR FORCE SYSTEMS COMMAND
# ARNOLD AIR FORCE STATION, TENNESSEE

# NOTICES

# TURBULENT WAKE AND SHOCK SHAPE
# OF HYPERVELOCITY SPHERES

A. B. Bailey

ARO, Inc.

# FOREWORD

This technical report has been reviewed and is approved.

Conrad O. Forsythe
Captain, USAF
Aerospace Sciences Division
DCS/Research

Donald R. Eastman, Jr.
DCS/Research

## ABSTRACT

Experiments have been conducted to study some of the properties of the inner turbulent wake behind high speed spheres in free flight over a wide range of velocity and pressure. Schlieren and shadowgraph techniques have been used to photograph the wake. It has been shown that the growth of the inner wake close to the body is a function of velocity and ambient pressure. In the very far wake ($x/d > 1000$) it has been shown experimentally that wake growth follows a 1/3 power law independent of velocity and ambient pressure. Experimental measurements of the location of transition from laminar to turbulent flow in the inner viscous wake have been shown to be dependent upon unit Reynolds number. Approximate axial velocity distributions in the inner viscous wake have been measured with oblique doppler radar techniques and a schlieren/drum camera system. These two systems measure such widely different velocities that it has been concluded that they measure the velocity at different radial positions in a wake which has strong radial gradients in velocity. Finally, a study of the shock shape for spheres for a wide range of pressure and velocity has shown that the shape is dependent upon Mach number rather than velocity and is independent of ambient pressure. This comment does not apply to the stand-off distance.

# CONTENTS

# ILLUSTRATIONS

## NOMENCLATURE

| | |
|---|---|
| A | Cross-section area $\pi d^2/4$ |
| a | Constant (Eq. (2)) |
| $C_D$ | Drag coefficient |

| | |
|---|---|
| d | Diameter |
| $J_0$ | Constant (Eq. (1)) |
| K | Constant (Eq. (2)) |
| $M_\infty$ | Free-stream Mach number |
| n | Constant (Eq. (2)) |
| $p_\infty$ | Free-stream pressure |
| $Re_\infty d$ | Free-stream body Reynolds number |
| $Re_\infty/in.$ | Free-stream unit Reynolds number |
| $Re_\infty x_{tr}$ | Transition Reynolds number |
| $V_W$ | Wake velocity |
| $V_\infty$ | Free-stream velocity |
| w | Turbulent inner wake width |
| $w_1$ | Inviscid wake width |
| x | Axial distance |
| y | Radial distance |
| $\gamma_\infty$ | Free-stream specific heat ratio |
| $\lambda$ | Neck enthalpy/stagnation enthalpy |
| $\lambda_1$ | Constant (Eq. (1)) |

# SECTION I
## INTRODUCTION

Investigations of the wakes generated by high speed bodies at remote distances from the body have assumed some importance in recent years. The reason for this is that the trail a body leaves behind it is a function of the body shape, size, ambient pressure, and velocity. This trail is considered to be a source of observables which can be used to identify the body. Some methods of observing the trail of a re-entering body depend upon the radar reflection from the wake. The interaction of the electromagnetic wave with the trail can be shown to be influenced by the electron density, collision frequency, wake width, and the laminar or turbulent nature of the flow. These electrical properties can be proven to be sensitive to contamination from the injection of some foreign gas or the products of ablation.

In an aeroballistic range, it is possible to study the trails far behind bodies at the ambient pressure and velocity which duplicate the full-scale vehicle trajectory. However, because of the small scale of the model generally the nonequilibrium effects cannot be simulated. The effect that this lack of true simulation has on fluid dynamic properties such as wake velocity, wake growth, and transition from laminar to turbulent flow is not completely clear at this time.

Wakes of both slender and blunt bodies have been studied in aeroballistic ranges using shadowgraph and schlieren techniques. A blunt body traveling at hypersonic speeds is typified by the following three main flow regimes (Fig. 1):

1. The detached bow shock wave which is almost normal in the stagnation region of the body

2. An essentially inviscid, high temperature outer wake composed of gas which has passed through the strong, curved portion of the bow shock, i.e., an "entropy wake"

3. The viscous, high temperature inner wake generated by the body boundary layer

Slender bodies give rise to the same flow regimes but, because of the much weaker bow shock wave, the inviscid shock layer is both cooler and narrower, and, because of the thicker body boundary layer, the inner viscous wake is more pronounced. Thus, the blunt body can be considered to generate a shock dominated trail, whereas the slender body generates a boundary-layer dominated trail. Because of the basic differences in the wakes of these types of body, it is reasonable to

assume that the interaction of an electromagnetic wave with a body trail will be a function of body shape. If we consider both a spherical and a slender body at 150,000 ft altitude traveling at 23,000 ft/sec, the electron densities 100 body diameters behind these bodies are of the order of $10^{11}$ and $10^8$ electrons/cc, respectively, assuming that the wake is laminar in both cases.

There is interest in determining the point at which transition from laminar to turbulent flow occurs for a range of body shapes, sizes, velocities, and ambient pressures. It is conjectured that the radar reflections from laminar and turbulent wakes will be sufficiently different to make the determination of the transition region possible with a ground-based radar.

During the last few years, a body of information has been accumulated at the von Kármán Gas Dynamics Facility (VKF) on the properties of wakes behind spheres for a range of velocities, model sizes, and ambient pressures. Some limited data on the interaction of an electromagnetic wave with a sphere wake have also been obtained under certain flight conditions using focused, 35-kmc microwave probes.

## SECTION II
## APPARATUS

### 2.1 TEST CELL

A complete description of the hypervelocity pilot range (Armament Test Cell, Hyperballistic (K)) can be found in Ref. 11. Briefly, Range K (Fig. 2) consists of the following components: launcher, blast and range tanks, and instrumentation.

### 2.2 LAUNCHER

The launcher is a two-stage, light-gas gun (Fig. 2) consisting of a combustion chamber, pump tube, high pressure section, and launch tube. Various high pressure sections and launch tubes ranging in diameter from 0.375 to 1.0 in. have been used with this launcher.

In order to protect the model in the launch tube, it is mounted in a plastic sabot (Lexan®). Two main types of sabot have been used in the present work (Fig. 3).

## 2.3 BLAST AND RANGE TANKS

Both of these tanks are 6-ft-diam cylinders joined by a short spool piece (Fig. 2) containing a high vacuum valve which permits the isolation of the two tanks.

The blast tank is 12 ft long and has a series of ports along the sides and upper surface to permit X-ray photographs to be taken of the model and sabot after they have left the launch tube (Fig. 4). The range tank is 103 ft long and is equipped with six dual-axis shadowgraph stations installed at approximately 15-ft intervals.

## 2.4 INSTRUMENTATION

### 2.4.1 Range Instrumentation

A complete description of pressure, temperature, and velocity measuring techniques is given in Refs. 1 and 2, together with a description of the model detectors.

### 2.4.2 Flow Field Visualization Instrumentation

In a turbulent flow, although the density fluctuations are small because the turbulent cell size is also small, the first and second derivatives of density can be large. Since the shadow method of flow visualization is sensitive to the second derivative of density, it is therefore inherently sensitive to measurements of turbulence. The existing Fresnel lens shadowgraph system, although not designed specifically for flow visualization, offers possibilities of studying the turbulent wake at each of the six orthogonal stations in any one launching. A typical turbulent wake shadowgraph obtained with the Fresnel lens system is shown in Fig. 5.

A high quality single-pass schlieren system exists to study body flow fields over a wide range of model flight conditions. A schematic drawing of the Range K schlieren system is shown in Fig. 6. This is basically a twin concave mirror system with a field of view of approximately 12 in. This system can be operated with a vertical or horizontal knife edge, a vertical or horizontal Wollaston prism, or as a focused shadowgraph system. A Speed Graphic® camera is used with a single flash spark source. When the multispark Strobokin light source is used, a high speed drum camera provides as many as twenty photographs of the model flow field. Either of these cameras can be used with any of the optical systems. For low ambient pressures, it is necessary to use

a knife-edge system in order to utilize to the fullest the sensitivity of the schlieren system. This requires a high degree of schlieren structural stability. The schlieren system is located in a region containing some heavy rotary equipment, and this has necessitated the development of a servocontrolled knife-edge positioner. This system has been shown to be capable of compensating for any of the vibrations associated with the above equipment. Before the development of the servo knife-edge system, a Wollaston prism which, depending upon the manner of mounting, can be made to simulate a vertical or horizontal knife edge, has been used in place of the knife edge. This results in a reduction in sensitivity as compared to the knife edge and the formation of two closely overlapping images. However, both of these disadvantages are more than offset by the fact that the whole system is insensitive to vibration. In Fig. 5, the schlieren, used as a focused shadowgraph, is compared to a Fresnel lens shadowgraph. For the very far wakes, the shadowgraph system is inadequate and a more sensitive system has to be used. In Fig. 5, a photograph of the very far wake using the Wollaston prism is shown. A photograph of the far wake of a sphere using the servocontrolled knife edge is shown in Fig. 7.

### 2.4.3 Microwave Instrumentation

Some attempts have been made to study oblique scattering from the ionized wakes of spheres with an oblique focused 35-kmc microwave beam. The antenna is located in the range tank and is mounted at an angle of 45 deg to the longitudinal axis of the range. It is focused to a diameter of approximately 2 in. at the range centerline. All the equipment associated with this system is located outside the range tank. The backscattered signal is recorded on oscilloscopes which are triggered by a shadowgraph station detector with a delay determined by the model velocity.

## SECTION III
## DISCUSSION OF EXPERIMENTAL RESULTS

### 3.1 TURBULENT WAKE GROWTH

The position of the body with respect to the portion of the wake in the schlieren or shadowgraph field of view is determined in the manner suggested by Slattery and Clay (Ref. 3). The velocity of the projectile as it travels past the optical station is measured together with the delay time between passage through the station and the firing of the station spark source. The distance behind the model of the section of wake

photograph is said to be given by the product of the velocity through the station and the delay time as defined above. For the present series of launchings, when the schlieren system alone was being used to study the wake, the velocity through the schlieren station can be accurately interpolated from the velocity-distance data obtained with the six orthogonal shadowgraph stations. The time delay between the passage of the projectile and the firing of the spark source was measured with a 10-mc interval counter. For the higher pressure firings ($p_\infty \geq 200$ mm Hg), where some of the Fresnel lens shadowgraph stations were used to photograph portions of the model wake, the velocity and time delays were interpolated from the velocity-distance and velocity-time data provided by the stations used to photograph the model only.

Because of the conical light rays from the Fresnel lens shadowgraph spark source, there is some magnification of the model in the Fresnel lens plane. As a result of detailed calibrations of each of the orthogonal shadowgraph stations, the true size of the sections of wake photographed can be measured. (These calibrations have indicated that the magnification is on the order of 1.5.)

Wake widths have been derived by tracing the boundary of the turbulent core with a planimeter and averaging the width over a distance of at least ten body diameters for values of $x/d \geq 100$. For the higher pressure firings for which orthogonal shadowgraphs of the wake were obtained, it was noted that there was some evidence of asymmetry in the wake. However, because a much larger number of photographs than were obtained in the present series of launchings would be required to make a firm conclusion as to the degree of this asymmetry, for the present work the data obtained from the orthogonal photographs have been averaged. In making measurements of the turbulent wake width in the very far wake ($x/d \geq 1000$), small models have been used. This was necessary for two reasons: (1) the field of view of the present schlieren system (approximately 12 in.) was too small to enable study of the sizes of the turbulent far wakes of large models and (2) the turbulent core did not grow in a smooth manner but grew in a cyclic manner, where the distances between the points of greater diameters are a function of the model size. This means that, if the optical field of view is too small, the wake width can be averaged only over a section of maximum or minimum width. This problem is illustrated by the photograph of the very far wake of a 1/8-in.-diam sphere in Fig. 9. The ratio of the maximum to minimum width in this photograph is on the order of 1.5. This problem of compatibility of field of view size and the size of the model under study has been discussed by Braun in Ref. 4. In fact, his recommendation is that the field of view should cover several cycles of this quasi-cyclic formation.

The experimental data obtained at the VKF cover the pressure range from 10 to 600 mm Hg over the velocity range from 7000 to 21,000 ft/sec. Some photographs of turbulent wakes are shown in Figs. 10 through 13. Values of wake width derived from these and other photographs are plotted in Figs. 14 through 18. Wake width and axial distance are expressed in terms of the parameters $w/\sqrt{C_DA}$ and $x/\sqrt{C_DA}$, as suggested in Ref. 5. In correlating the data obtained in the present tests, the values of $C_D$ used were consistent with the values given in Ref. 1. Where data from various sources are compared using these parameters, if no value for $C_D$ was quoted in the reference, the values given by Ref. 1 were used in the calculation of the parameters.

A comparison of the present data at a pressure of 600 mm Hg with data obtained in other facilities at atmospheric pressure is shown in Fig. 14. Very good agreement is indicated with Kynstautas' (Ref. 6) data obtained for a 3-in.-diam sphere and that obtained in the present tests for spheres less than 1 in. diameter. Data obtained at slightly lower velocities at atmospheric pressure (Refs. 4, 7, and 8) although not shown in Fig. 14 are also in good agreement with the present data and those of Ref. 6. The theoretical predictions of Lees and Hromas (Ref. 9) and Lykoudis (Ref. 10) are also in good agreement with these experimental data. The experimental data presented in Ref. 3 are shown in Fig. 14. These indicate a larger wake than either of the theories or the experimental work. No explanation can be found at this time for this difference.

In Fig. 15 some experimental data obtained at an almost constant velocity but with varying ambient pressure are compared with theories of Refs. 9 and 10. The experimental results indicate a small but consistent trend of an increase in wake width at a fixed axial station with reduction in ambient pressure for $x/\sqrt{C_DA} \leq 1000$. This trend is consistent with an increase in the ratio of neck enthalpy to stagnation enthalpy. Both theories are based on the same physical considerations, and both depend on the initial conditions chosen for the wake calculations. The theory of Ref. 9 requires extensive numerical calculations and results of only two cases calculated by this theory were published. Lykoudis (Ref. 10), although starting from the same basic assumptions, has made a series of approximations which give a closed form solution. This has permitted a study of the effect of Mach number and neck enthalpy on wake growth. Both theories are in agreement that for $x/\sqrt{C_DA} \geq 1000$, the wake growth is independent of Mach number and neck enthalpy.

In Fig. 16, some data obtained at slightly higher velocity at a pressure of 300 mm Hg are shown. One of the conclusions possible from

Fig. 15 is that for pressures such as this, a neck-to-stagnation enthalpy ratio near 0.5 should be applicable. It can be seen that this curve does approximate the experimental results reasonably well.

For velocities greater than 10,000 ft/sec, there is a relatively small body of published information on the growth of the turbulent inner wake. At AVCO, NOL, and M.I.T., (Refs. 5, 11, and 12, respectively) data on wake growth for velocities between 15,000 and 20,000 ft/sec have been obtained with shadowgraph, schlieren, and luminosity techniques. It can be seen in Fig. 17 that the experimental shadowgraph and schlieren data from these various sources are in reasonable agreement. On the basis of the trend shown in Fig. 15, it would be expected that the low pressure data, $p_\infty = 35$ mm Hg, would agree with Lykoudis' theory for a neck-to-stagnation enthalpy ratio greater than 0.5. The present results indicate that this is true (Fig. 17). With present experimental techniques, it has been found impossible to obtain measurements of the inner turbulent wake width for $x/\sqrt{C_D A} \le 90$. The reason for this can be seen by referring to Fig. 12. It is evident that for conditions such as those in Fig. 12, the inner turbulent wake is completely embedded in the inviscid wake and is thus invisible to examination by schlieren techniques. On the basis of the experimental results to date, it would appear reasonable to conclude that Lykoudis' (Ref. 10) prediction of the form of the wake growth in the near wake is in better agreement with experiment than is the prediction of Lees and Hromas (Ref. 9).

A technique used at AVCO (Ref. 5) to study the growth of the turbulent inner wake is to fire plastic projectiles which ablate strongly and give rise to a highly luminous wake. It is considered that the products of ablation act as a dye and correctly delineate the boundary of the viscous wake. Three techniques, involving an image converter camera, a race track camera, and a wake scanner instrument, were used to obtain wake growth data out to values of $x/d = 1200$. Complete details of these techniques are given in Ref. 5. In the course of the present study, a highly ablating nylon sphere (Fig. 13) was launched, and the measured wake width was greater than measured at AVCO for the bluff body, at least where the two sets of data overlap (Fig. 17).

Many attempts have been made to demonstrate the 1/3 power law dependence of wake growth. In Refs. 9 and 10 it is indicated that such a dependence is true in the far wake and that there is no velocity dependence in this region. A comparison of all the available experimental data for $x/\sqrt{C_D A} \ge 1000$ is made in Fig. 18. Although these data cover a wide velocity range (7000 to 21,000 ft/sec) and a large ambient pressure range (15 to 600 mm Hg), a 1/3 power law dependence of $w/\sqrt{C_D A}$ is indicated by these data, which have a scatter on the order of ±20 percent at a fixed value of $x/\sqrt{C_D A}$.

## 3.2 TRANSITION FROM LAMINAR TO TURBULENT FLOW

One of the problems in correlating wake-transition data is that, at this time, no correlation parameters have been derived which fully account for the effects of body shape on transition. Several attempts have been made to correlate all the available wake transition data and an example of this, given by Zeiberg (Ref. 13), is shown in Fig. 19. The purpose of this correlation is to provide a simple formula for the prediction of wake transition for full-scale hypersonic re-entry bodies. Although this correlation employs concepts which have been successfully used in correlating boundary-layer and free-shear-layer transitions, there are uncertainties (Ref. 14) concerning its validity when used to predict transition for large bodies.

In the present discussion, only sphere wake transition will be considered. Previous experience (Ref. 14) has shown that, for a fixed body shape, transition is a function of Mach number and a Reynolds number (for simplicity free-stream Reynolds number will be used). An examination of Zeiberg's correlation (Fig. 19) indicates that, for $M_\infty = 7.5$ and for a unit Reynolds number range from 0.4 to 11 x $10^5$ in.$^{-1}$, the transition Reynolds number of sphere wakes varies from $10^6$ to $10^7$. Implicit in Zeiberg's correlation is the assumption of a unique transition Reynolds number for a fixed free-stream Mach number and body shape. On the basis of available data, including the present, it is reasonable to conclude that transition distance also is a function of unit Reynolds number. This possibility is suggested by Erdos and Gold (Ref. 14). (It is of interest to note that boundary-layer transition on many different shapes has been shown to be a function of unit Reynolds number. For example, see Refs. 15 through 17). All of the available ballistic range data on spheres together with data obtained in the present study are shown in Figs. 20 and 21.

In Fig. 20, data obtained at velocities on the order of 8000 ft/sec are presented. For a sphere diameter of 0.5 in. where data from the present tests overlap with those obtained by Clay and Slattery (Ref. 3), there is good agreement in the region of overlap. A unit Reynolds number range from 5 x $10^4$ to 4 x $10^6$/in. is covered by these two sets of data. As the unit Reynolds number decreases initially, the transition Reynolds number decreases until, at a unit Reynolds number of approximately 2 x $10^5$/in., the transition Reynolds number possibly undergoes an increase with further decrease in unit Reynolds number. The data for the 0.125-in.-diam sphere seem to indicate a similar behavior. For this sphere size however, the unit Reynolds number at which the transition Reynolds number is a minimum, is now approximately 9 x $10^5$/in. The data obtained for the 0.25-in.-diam sphere indicate a

minimum transition Reynolds number between the 0.125- and 0.5-in.- diam values, but the suggested increase in transition Reynolds number for lower values of unit Reynolds number is not as well defined. Also plotted in Fig. 20 are the results of some transition measurements made on the surface of a large hollow cylinder parallel to a hypersonic wind tunnel flow (Ref. 15) and on an ogive-cylinder parallel to a supersonic wind tunnel flow (Ref. 16).

It can be seen that, in the unit Reynolds number range of this experiment ($4 \times 10^5$ to $3 \times 10^6$/in.), the transition Reynolds number varies in the same manner as for the sphere wakes. Demetriades and Gold (Ref. 18) have obtained some data on the transition from laminar to turbulent flow in the wake of a transverse cylinder. A curve representing the best average through their experimental data is shown in Fig. 20. Although these results cover a small range of unit Reynolds number, they do indicate that as the unit Reynolds number is reduced, at small values of unit Reynolds number, the transition Reynolds number increases. This variation is in agreement with that indicated by some of the data obtained for spheres (Fig. 20) and does suggest that at low unit Reynolds numbers there may be an abrupt increase in transition Reynolds number.

In Fig. 21 all the available high speed (15,000 to 26,000 ft/sec) wake transition data are plotted. The data obtained for the high speeds are not as comprehensive as for the lower speeds. However, the data of Refs. 12 and 19 and the present data for the 0.25-in.-diam models indicate the same general trend as at the lower speed. Photographs of what was considered to be transition in the wake of a high speed, 0.25-in.-diam sphere are shown in Figs. 22a and b. Photographs taken from either side of the axial station in the photograph in Fig. 22a were, respectively, laminar and turbulent. The bar placed on this data point in Fig. 21 indicates the distance spread covered by the photographs. The form of this phenomenon is demonstrated in Fig. 22b where a sequence of drum camera photographs of the wake of a high speed sphere at low pressure are shown. It is of interest to note that these two data points obtained at low unit Reynolds numbers lie between the level of transition Reynolds numbers measured in the present work and those of Refs. 12 and 19.

In the foregoing discussion no mention has been made of the problems of determining when transition from laminar to turbulent flow has occurred in the wake. As mentioned earlier, the wake behind a sphere is composed of two parts: (1) the high temperature outer wake generated by the passage of the gas through the curved, strong part of the bow shock wave and (2) the high temperature, viscous, inner wake generated by the boundary layer. The density gradients in the inner and outer

wakes make it difficult to distinguish between the two regions. This in turn makes it difficult to determine the position of transition from laminar to turbulent flow in the inner viscous wake. This problem is well illustrated in Figs. 11 and 12. For the high speed case in Fig. 12, it can be seen that at 80 body diameters behind the sphere the viscous inner wake cannot be identified within the inviscid outer wake. For the succeeding photographs in this sequence the turbulent inner wake can be seen breaking through the inviscid outer wake and giving rise to a weak shock wave system. It seems reasonable to conclude that these shock waves are generated by the turbulence in the viscous inner wake. Returning now to the photograph at 80 body diameters behind the sphere, it can be seen that, although the inner turbulent wake is not visible, it is reasonable to conclude that it is turbulent because of the existence of the shock waves between the body bow shock and the inviscid outer wake. For the high speed cases where it has not been possible to distinguish between the inner and outer wakes, the point of transition has been determined by the position of these shock waves. That this is a reasonable method of defining transition in the inner wake is evidenced by the good agreement between the present results and those obtained elsewhere. However, at low pressures (e. g. Figs. 22a and b) these weak shock waves are not discernible, and it becomes difficult to determine the position of transition. It has been suggested that the data of Ref. 12 in Fig. 21 represent the position at which the turbulent inner wake breaks through the inviscid outer wake, (not necessarily the location of transition in the inner wake). The fact that most data in Figs. 22a and b show turbulence orders of magnitude sooner than do the data of Ref. 12 encourages the belief that the lower $Re_{\infty}x_{tr}$ represents transition of the inner viscous wake.

Webb et al. (Ref. 20) suggest that, provided the free-stream Mach number is large, then transition is independent of Mach number. Examination of Figs. 20 and 21 indicates that indeed the transition Reynolds number is a weak function of Mach number. Wilson (Ref. 19) suggests that this weak dependence can be accounted for by using $(Re_{\infty}x_{tr})/M_{\infty}$ as the correlating parameter. Accordingly, all the available sphere wake data in the Mach number range of 5 to 20 are plotted in Fig. 23. Examination of this figure shows that the bulk of the experimental data falls within a ±30-percent band. For body Reynolds numbers less than $4 \times 10^4$, the transition distance appears to increase very rapidly. This rapid increase in transition distance is based on seven data points, four low speed ($M_{\infty} = 7.5$) and three high speed($15 \leq M_{\infty} \leq 21$). For the case of the VKF high speed shot (Fig. 22a), the inviscid wake has a diameter of approximately eight body diameters, whereas the corresponding turbulent wake would have a diameter of approximately nine body diameters at this axial distance behind the sphere. Transition in

the wake of a free-flight, 8-in.-diam sphere has been derived from a doppler analysis of the radar return (Ref. 12) and is plotted in Fig. 23. At this measured transition distance, it can be shown that both the inviscid and turbulent wake diameters are approximately equal to 16 body diameters. This tends to support the suggestion that the transition values quoted in Ref. 12 are in fact the points at which the turbulent inner wake emerged from the inviscid outer wake. This type of transition seems to be significant since it apparently may be this point of breakthrough which provides a backscattered radar return. From a consideration of re-entry detection, this event may be of more significance than transition from laminar to turbulent flow in the viscous inner wake, since this latter phenomenon often cannot be detected either with a radar system or a schlieren system. Of course another possibility is that Figs. 22a and b represent some form of apparent transition to turbulence in the outer inviscid wake. This introduces an element of doubt into the interpretation of these seven data points. Wilson (Ref. 19) has shown that the inviscid outer wake growth can be expressed in the form

$$w_i/d \sim (x/d/Re_\infty d)^{1/4}$$

Wilson's data, together with some data obtained in the VKF in the same speed range, are shown in Fig. 24.

The effects of unit Reynolds number and body Reynolds number on transition Reynolds number are of importance since to date it has usually been assumed that transition Reynolds number in wakes is a function of Mach number only for a particular body shape (Ref. 13).

## 3.3 WAKE VELOCITY

Two techniques have been used to measure the velocity of the turbulent wake behind a sphere. A repetitive light source, whose frequency can be as high as 10 kc, permits, in conjunction with a high speed drum camera, as many as twenty photographs of the turbulent wake of a model to be taken. In Figs. 10 and 13, photographs obtained with this system are shown. For the low speed shot, it is possible to follow a particular turbulent cell on the periphery of the wake through several frames and, from a knowledge of the time between frames and the distance moved, the cell velocity can be calculated. For the high speed shot where the pulse frequency of the spark source was much slower (i.e., on the order 2 kc), the motion of individual turbulent cells is too slow to be measured with any accuracy with this technique.

The other method used to measure wake velocity is the oblique focused doppler radar. With this system, if the electron density in the

wake of a nonablating body is sufficiently high, then the incident micro-
wave energy will be reflected. If the regions of high electron density
can be assumed to be directly related to the fluid dynamic properties of
the turbulent wake then such a method should give a measure of the
axial velocity variation in the wake of a body. In the present series of
tests where the projectile velocity has been less than 21,000 ft/sec,
wake electron density measurements (Refs. 12 and 21) have shown that
with the 35-kmc system used here, reflection from the clean wake would
not be expected. However, small amounts of model ablation can be
shown to provide a highly reflective wake. A good example of this is
given in Fig. 25 where an ablating steel sphere is compared with a non-
ablating tungsten carbide sphere at similar flight conditions. For the
ablating steel sphere (Fig. 25a) there is a strong signal from the wake,
whereas the nonablating tungsten model (Fig. 25b) gives no reflection.
(It is of interest to note that a ballistic spectograph indicated the pre-
sence of iron in the steel sphere flow field.) Bearing in mind that
microwave signals can behave in different ways depending on the mate-
rial in the wake, the tungsten carbide sphere was fired at atmospheric
pressure where it gave a strong wake reflection (Fig. 25c). From the
foregoing it is reasonable to assume that model material contamination
in the wake provides a reflecting surface for the microwave energy.
This is analogous to the technique used by AVCO (Refs. 4 and 22) to
delineate the extent and velocity of a turbulent wake by studying the
luminosity generated by a highly ablating plastic model. It has been
shown in an earlier section that the luminous turbulent wake measured
in this manner is not the same as that measured optically (i.e. from
schlieren and shadowgraph photographs). Therefore, in any application
or comparison of the measured wake velocities of ablating bodies it must
be remembered that these velocities may not be truly representative of
the fluid velocity, at least in the outer part of the wake.

In Fig. 26, the velocity distribution obtained with the present tech-
niques is compared with measurements made at M.I.T., AVCO, and GM
(Refs. 3, 22, and 23) and also with the theoretical variation (Ref. 9).
The present focused oblique doppler radar results are in very good agree-
ment with those obtained at GM (Ref. 23) and also with the theory. Five
different contaminants, nylon, copper, tungsten carbide, aluminum, and
steel, have been injected into the wakes by ablation. These five mate-
rials represent a range in specific gravity from approximately 1 to 15
and a melting temperature range from 500 to 3500°K. For this wide
range of material properties, no consistent effect upon the wake velocity
can be detected. From this it appears reasonable to conclude that the
degree of contamination is not large enough to significantly modify the
fluid dynamic properties of the wake. As noted earlier, the diameter
of the turbulent wake of an ablating nylon sphere was slightly larger

(approximately 10 percent than that of a clean wake (Fig. 17). However, this cannot be considered conclusive because normally scatter of this order of magnitude is inherent in such measurements. Therefore, the wake velocities measured in this manner should closely approximate the clean wake velocity, and this presumably contributes to the good agreement with the theoretical values.

The wake velocity measured from the motion of a peripheral turbulent cell indicates either that there is a very strong effect of projectile velocity on the decay in the wake or that there are very pronounced radial velocity gradients in the wake. For example, at a distance of 300 body diameters from the body, the doppler radar-determined velocity ratio, $V_w/V_\infty$ is 0.1, whereas the schlieren-determined velocity ratio is on the order of 0.01. The present schlieren data are lower than those measured in this manner and reported in Ref. 3. Some data obtained with a drum camera at AVCO (Ref. 22) on the velocity of ablating particles in the wake of a body are also shown in Fig. 26. These results were obtained at a velocity close to that corresponding to the schlieren data obtained in the present tests. The AVCO data are in very good agreement with the oblique doppler radar, which would indicate a very weak influence of projectile velocity on the ratio of wake velocity to projectile velocity. The agreement in the region where these results overlap with the present schlieren results is not good. As noted in an earlier discussion, the measured luminous wake has a smaller diameter than that based on schlieren photographs. This probably means that the velocity measured from the luminous wake is at a station closer to the wake axis than the schlieren measured velocity. This would tend to confirm the existence of strong radial velocity gradients in the wake.

It is also interesting to note that the wave form of the doppler radar wake return is clean (Fig. 25) indicating that the reflection is from a relatively uniform source. The velocity measured by the oblique doppler radar does not represent a measurement of the average wake velocity, but rather it represents the velocity of the region in the wake which best reflects the radar energy. The good agreement between the measured luminous and radar wake velocities indicates that the contaminants which provide the source of luminosity and radar reflection are probably confined to the same region of the turbulent inner wake.

## 3.4 SHOCK WAVE PROFILES FOR SPHERES

A knowledge of the shock wave profiles is of interest since it is necessary as a starting point in the calculation of the flows over blunt-nosed bodies. Various authors have shown that the blast wave analogy

predicts the important features of hypersonic flow over blunt bodies.
It has been shown that the second-approximation blast analogy equation
for shock wave shape is exactly hyperbolic (Ref. 24), i.e.,

$$y/d = (\gamma_\infty C_D/4 J_0)^{1/4} (x/d)^{1/2} \left[ 1 - \lambda_1/M_\infty^2 (4 J_0/\gamma_\infty C_D)^{1/2} x/d \right]^{1/2} \tag{1}$$

where $\lambda$ and $J_0$ are functions of the free-stream specific heat ratio, $\gamma_\infty$.

An experimental program has been conducted in the Ames Super-
sonic Free Flight Wind Tunnel (Ref. 25), where data on the shock pro-
files of a series of ellipsoidal-nosed cylinders have been obtained in the
Mach number range 5 to 15. In this facility, the high Mach numbers are
obtained by launching projectiles into a $M_\infty = 3.0$ flow generated by a
standard wind tunnel nozzle operating at a total temperature of approxi-
mately 300°K with air. Consequently, a value of $M_\infty = 15$ may be
obtained by launching a projectile at a velocity of 8000 ft/sec into this
flow. With this technique a high Mach number can be generated without
also generating the high temperatures, and hence the real gas effects,
normally associated with such a Mach number. From this study, it was
concluded that shock wave profiles could be represented by an equation
of hyperbolic form, viz,

$$y/d = K \left[ (x/d)^{1/n} + a (x/d) \right]^n \tag{2}$$

which has its apex at the origin and k is the slope of the asymptote.

With some algebraic manipulation, Eq. (1) can be written in the
same form as Eq. (2) where the constants in Eq. (2) are defined by
Ref. 25, i.e.,

$$\left. \begin{array}{l} K = (-\lambda_1)^{1/2}/M_\infty \\[2mm] a = C_D^{1/2} M_\infty^2 / -\lambda_1 (4 J_0/\gamma_\infty)^{1/2} \\[2mm] n = 1/2 \end{array} \right\} \tag{3}$$

A substitution of the theoretical values for the quantities described in
Eq. (3) did not give a good prediction of the shock shapes reported in
Ref. 25. Therefore, the experimental data of Ref. 25 were fitted by a
least squares routine which resulted in a different set of values for the
parameters in Eq. (3). It was found that these parameters could be
expressed as functions of drag coefficient and free-stream Mach num-
ber, viz,

$$K = (M_{\infty}^2 - 1)^{-0.5} + 0.057\, C_D^{1.35}\, M_{\infty}^{-0.0687}$$

$$a = 0.56 \left[ C_D^{0.75}(M_{\infty}^2 - 1) \right]^{0.274 - 115 [ C_D^{0.75} (M_{\infty}^2 - 1)]^{-0.07}}$$

$$n = ( 0.646\ e^{-0.237\ C_D^{0.75}} )( C_D^{0.5}\ M_{\infty}^2 )^{-0.034}$$

$$(4)$$

Another frequently used shock wave shape prediction is that of Van Hise (Ref. 26) who has obtained computer solutions for various body shapes. He found that, for high Mach numbers ($M_{\infty} \geq 20$), the shock shapes for the various bodies studied could be approximated by

$$y'd = 0.98 \left[ x'd\ (C_D)^{1/2} \right]^{0.46} \tag{5}$$

These three theoretical predictions are compared with some measured results covering the velocity range from 3000 to 21,000 ft/sec and the pressure range from 0.7- to 200-mm Hg. For this wide range of pressure it can be seen that for velocities on the order of 20,000 ft/sec, shock wave shape (not standoff distance) is independent of pressure within the limitations of present measuring techniques. Furthermore, it is of interest to note that, although these conditions cover a regime where real gas effects could be expected to be significant, the agreement with the prediction of Ref. 25, which does not account for real gas effects, is very good. This indicates that the real gas effects do not modify the shock shape to a degree sufficient to be measured. For a velocity of approximately 10,000 ft/sec, the result of Ref. 25 is again in good agreement with the measured values.

## SECTION IV
## CONCLUSIONS

In a study such as this, which has been to some extent an assessment of the sensitivity of some of the instrumentation developed to study trail observables, it is difficult to draw many firm, final conclusions. Further work is planned to make better use of the equipment, now that a better appreciation of its performance capabilities is available.

However, on the basis of the results obtained to date, the following conclusions appear to be valid:

1. In the near wake, the inner turbulent wake growth with distance has been shown experimentally to be a function of ambient pressure and velocity.

2. In the far wake, the inner turbulent wake width has been shown to have a 1/3 power law dependence on distance, independent of velocity and ambient pressure.

3. Transition from laminar to turbulent flow in the inner wake has been shown to be a function of unit Reynolds number, at least at higher unit Reynolds numbers. At low unit Reynolds numbers the point of transition in the inner wake is difficult to determine, being obscured by the entropy layer or inviscid wake of the bow shock. Thus, it is not clear at this time whether or not the point of transition or the point at which the inner wake bursts through the inviscid wake is of more significance.

4. Wake velocity measurements with oblique doppler radar and schlieren techniques indicate strong axial and radial velocity gradients in the near wake.

5. At a given velocity, shock shape is shown to be independent of ambient pressure. This has been shown at velocities of 10,000 and 20,000 fps over a pressure range of 1 to 200 mm Hg.

## REFERENCES

1. Bailey, A. B. "Sphere Drag Measurements in an Aeroballistics Range at High Velocities and Low Reynolds Numbers." AEDC-TR-66-59.

2. Lukasiewicz, J., Stephenson, W. B., Clemens, P. L. and Anderson, D. E. "Development of Hypervelocity Range Techniques at Arnold Engineering Development Center." AEDC-TR-61-9 (AD258782), June 1961.

3. Slattery, R. E. and Clay, W. G. "The Turbulent Wake of Hypersonic Bodies." American Rocket Society 17th Annual Meeting and Space Flight Exposition, No. 2673-62, November 13-18, 1962.

4. Braun, Walter F. "Growth of the Turbulent Inner Wake behind Large Spheres at Supersonic Velocities." BRL MR-1597, September 1964.

5. Taylor, R. L., Melcher, B. W., II, and Washburn, W. K. "Measurements of the Growth and Symmetry of the Luminous Hypersonic Wake behind Blunt Bodies." AVCO-Everett Research Laboratory Research Report No. 163, BSD TDR-63-108, May 1963.

6.  Kynstautas, R. "The Growth of the Turbulent Inner Wake behind a 3-in.-diam Sphere. CARDE-TR-488/64, January 1964.

7.  Dana, T. A. and Short, W. W. "Experimental Study of Hypersonic Turbulent Wakes." Convair Rep. ZPh-103, May 1961.

8.  Murphy, C. M. and Dickinson, E. R. "Growth of the Turbulent Wake behind a Supersonic Sphere." AIAA Journal, Vol. 1, No. 2, February 1963. pp. 339-342.

9.  Lees, Lester, and Hromas, Leslie. "Turbulent Diffusion in the Wake of a Blunt-Nosed Body at Hypersonic Speeds." J. A. S., Vol. 29, No. 6, August 1962. pp. 976-993.

10. Lykoudis, P. "The Growth of the Hypersonic Turbulent Wake behind Blunt and Slender Bodies." RAND RM-3270-PR, January 1963.

11. Lyons, W. C., Jr., Brady, J. J., and Levensteins, Z. J. "Hypersonic Drag, Stability, and Wake Data for Cones and Spheres." AIAA, No. 64-44. Aerospace Sciences Meeting, January 20-22, 1964.

12. Clay, W. G., Labitt, M., and Slattery, R. E. "Measured Transition from Laminar to Turbulent Flow and Subsequent Growth of Turbulent Wakes." AIAA Journal, Vol. 3, No. 5, May 1965, pp. 837-841.

13. Zeiberg, Seymour, L. "Correlation of Hypersonic Wake Transition Data." General Applied Sciences Laboratory Tech. Report No. 382, October 1963.

14. Erdos, John I. and Gold, Harris. "Comments on Transition Correlations for Hypersonic Wakes." AIAA Journal, Vol. 2, No. 9, September 1964. pp. 1675-1676.

15. Potter, J. Leith and Whitfield, Jack D. "Effects of Unit Reynolds Number, Nose Bluntness, and Roughness on Boundary-Layer Transition." AEDC-TR-60-5 (AD234478), March 1960.

16. Potter, J. Leith, Whitfield, Jack D., and Strike, William. "Transition Measurements and the Correlation of Transition Sensitive Data." AEDC-TR-59-4 (AD208775), February 1959.

17. Potter, J. Leith and Whitfield, Jack D. "Recent Developments in Boundary-Layer Research." AGARDograph 97, Part III, May 1965.

18. Demetriades, Anthony and Gold, Harris. "Transition to Turbulence in the Hypersonic Wake of Blunt-Bluff Bodies." ARS Journal, September 1962, pp. 1420-1421.

19. Wilson, L. N. "Body Shape Effects on Axisymmetric Wakes." General Motors Corporation TR-64-02K, October 1964.

20. Webb, W. H., Hromas, L., and Lees, L. "Hypersonic Wake Transition." AIAA Journal, Vol. 1, No. 3, March 1963. pp. 719-721.

21. Eschenroeder, A. Q. and Hayami, R. A. "Scaling Experiments on Wake Ionization behind Nonablating Hypersonic Spheres." General Motors Corporation TR-64-02L, November 1964.

22. Hidalgo, H., Taylor, R. L., and Keck, J. C. "Transition in the Viscous Wake of Blunt Bodies at Hypersonic Speeds." AVCO-Everett Research Laboratory Research Report 133, April 1961.

23. Primich, R. and Steinberg, M. "A Broad Survey of Free-Flight Range Measurements from the Flow about Spheres and Cones." General Motors Corporation TR-63-224, September 1963.

24. Lukasiewicz, J. "Hypersonic Flow-Blast Analogy." AEDC-TR-61-4 (AD259455), June 1961.

25. James, Carlton S. and Terry, James E. "Shock Wave Profiles over Elliposoidal-Nosed Bodies in Hypersonic Flow." J. A. Sc., September 1962, pp. 1128-1129.

26. Van Hise, Vernon. "Analytic Study of Induced Pressure on Long Bodies of Revolution with Varying Nose Bluntness at Hypersonic Speeds." NASA-TR-R-78, May 1961.
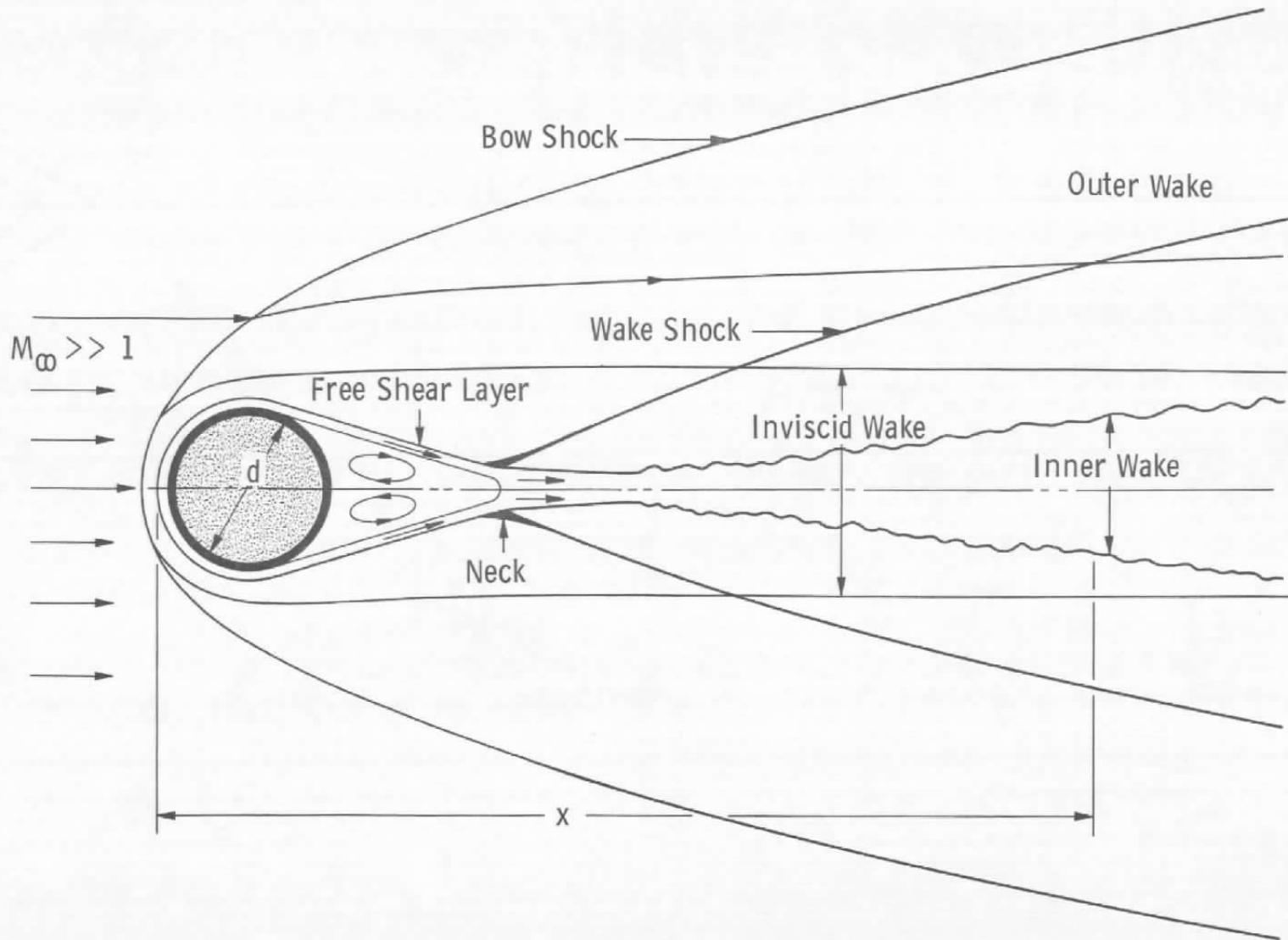
Fig. 1 Wake behind a Blunt Body at Hypersonic Speeds

RANGE TANK

RANGE ISOLATION VALVE

BLAST TANK

LAUNCHER BARREL

HIGH PRESSURE SECTION

PUMP TUBE

COMBUSTION CHAMBER

VACUUM
PUMPING
SYSTEM

TYPICAL SHADOWGRAPH STATION
(6 LOCATED AT 15 FOOT INTERVALS)

VACUUM PUMP
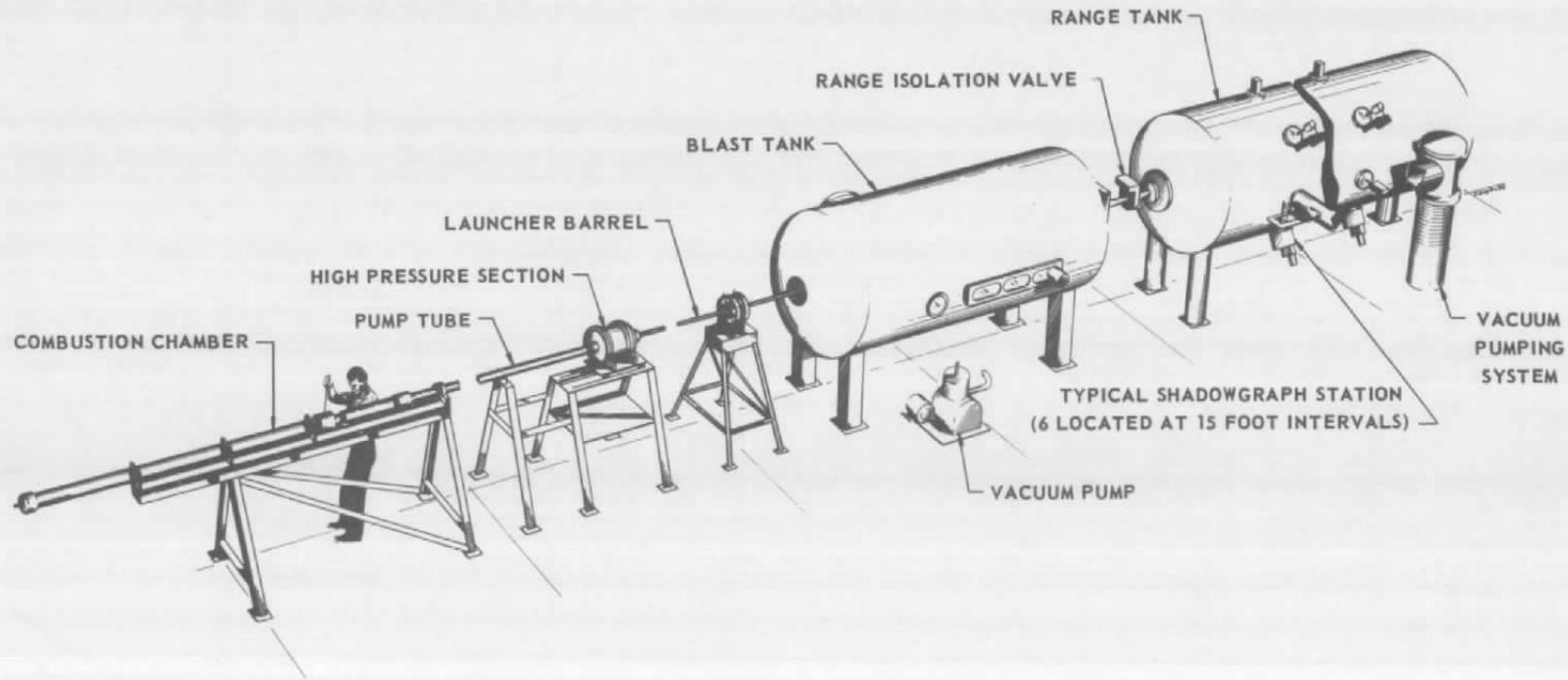
Fig. 2  Hypervelocity Range K
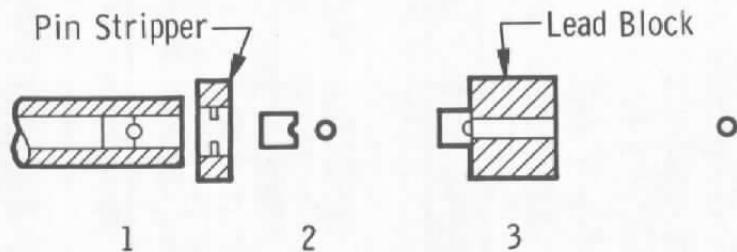
1. Model and Sabot Together in Launch Tube
2. Model and Sabot Separated after Passing through Pin Stripper
3. Sabot Arrested by Lead Block; Model Passes through a Hole in the Block and on Down Range

Pin and Lead Stripper
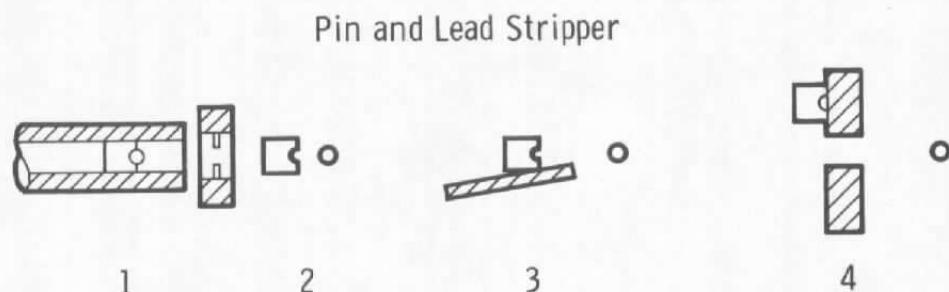


1-2. As Above
3. Sabot Strikes Angle Ramp and Deflects Vertically
4. Sabot Strikes Catcher Plate; Sphere Passes through Hole and on Down Range

Pin and Ramp Stripper
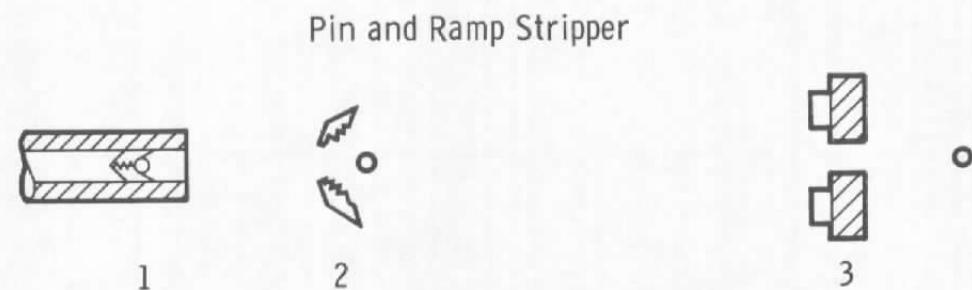


1. Model and Sabot Together in Launch Tube
2. Petalled Sabot Spreading under Action of Aerodynamic Forces
3. Sabot Arrested by Catcher Plate; Sphere Passes through Hole and on Down Range

Aerodynamic Stripper

Fig. 3 Model Separation Techniques Used in Range K
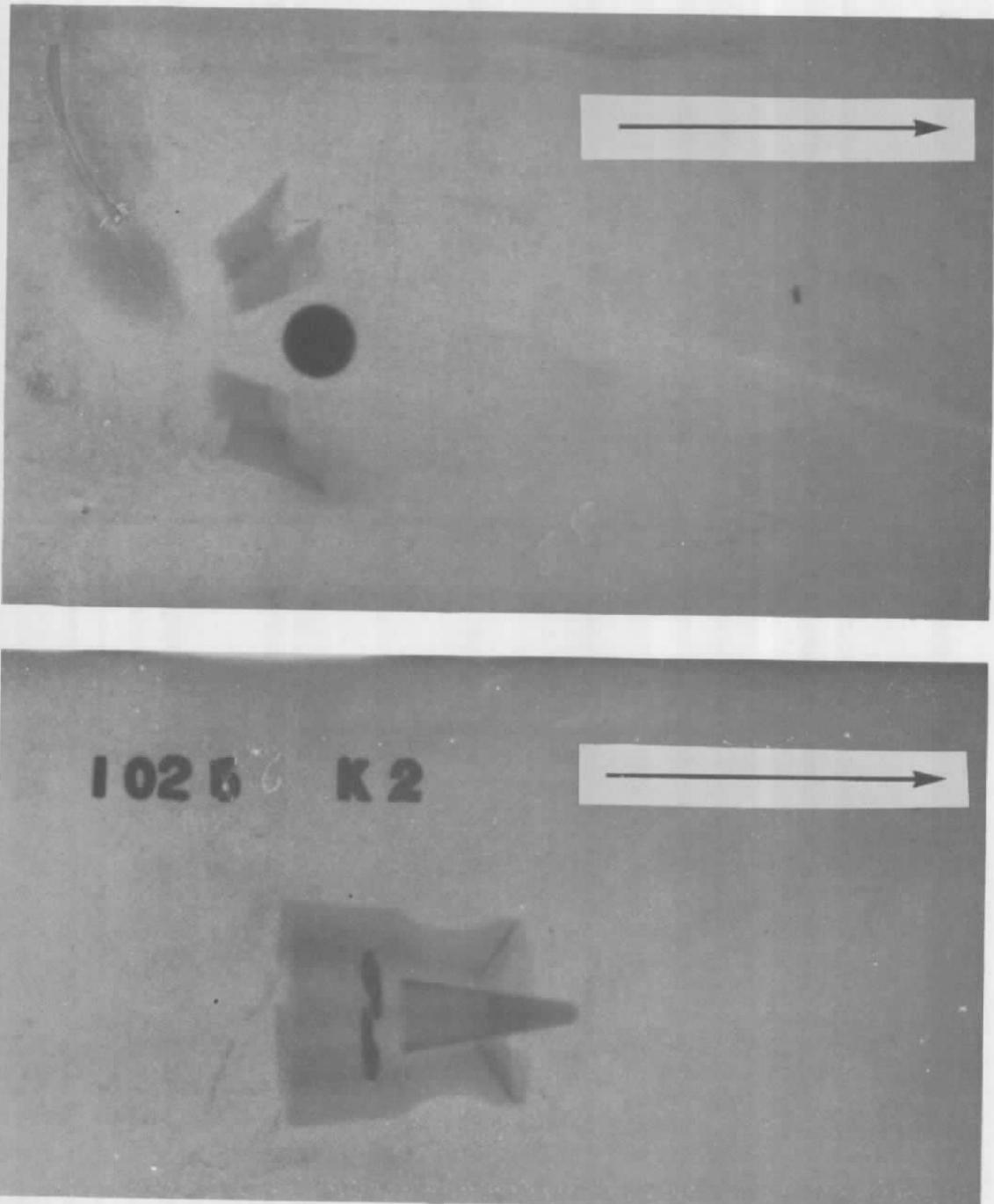
Fig. 4  X-Ray Shadowgrams

Fresnel Lens Shadowgraph, x/d = 512
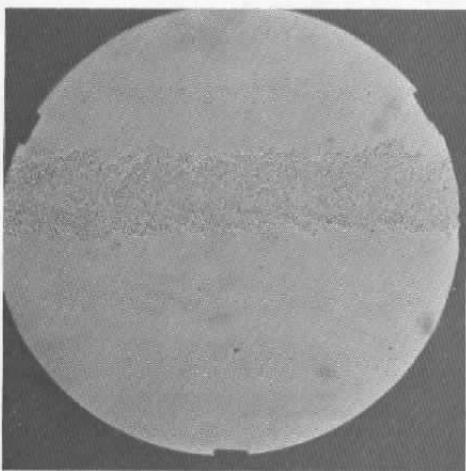


Schlieren Used as a Focused
Shadowgraph, x/d = 412
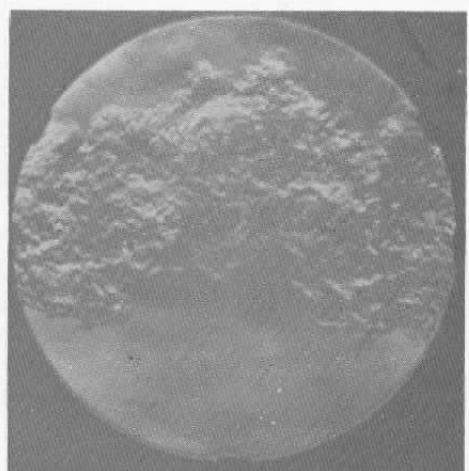


Schlieren Using Wollaston
Prism, x/d ≃ 20,000

Fig. 5 Turbulent Wake behind a Sphere at an Ambient Pressure
of 600 mm Hg (9000 $\leq V_\infty \leq$ 10,000 ft/sec)

Camera
Speed Graphic
or High Speed
Drum Camera

Lens

Knife Edge

Range Tank

High Quality
Schlieren Window

Concave Mirror

Slit

Lens

Spark Source Single Flash
or Multiflash Strobokin
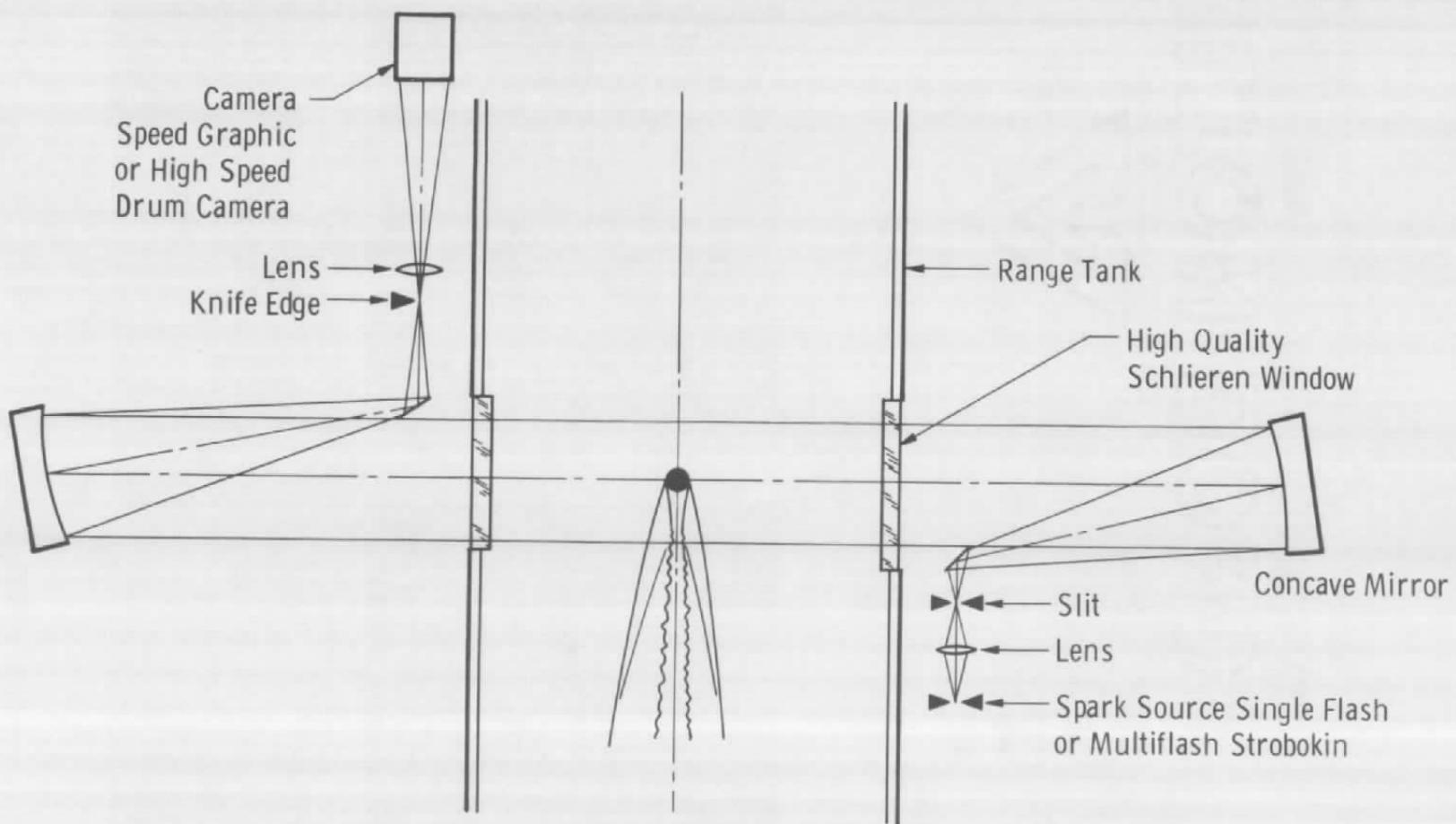
Fig. 6  Hypervelocity Range K Schlieren System
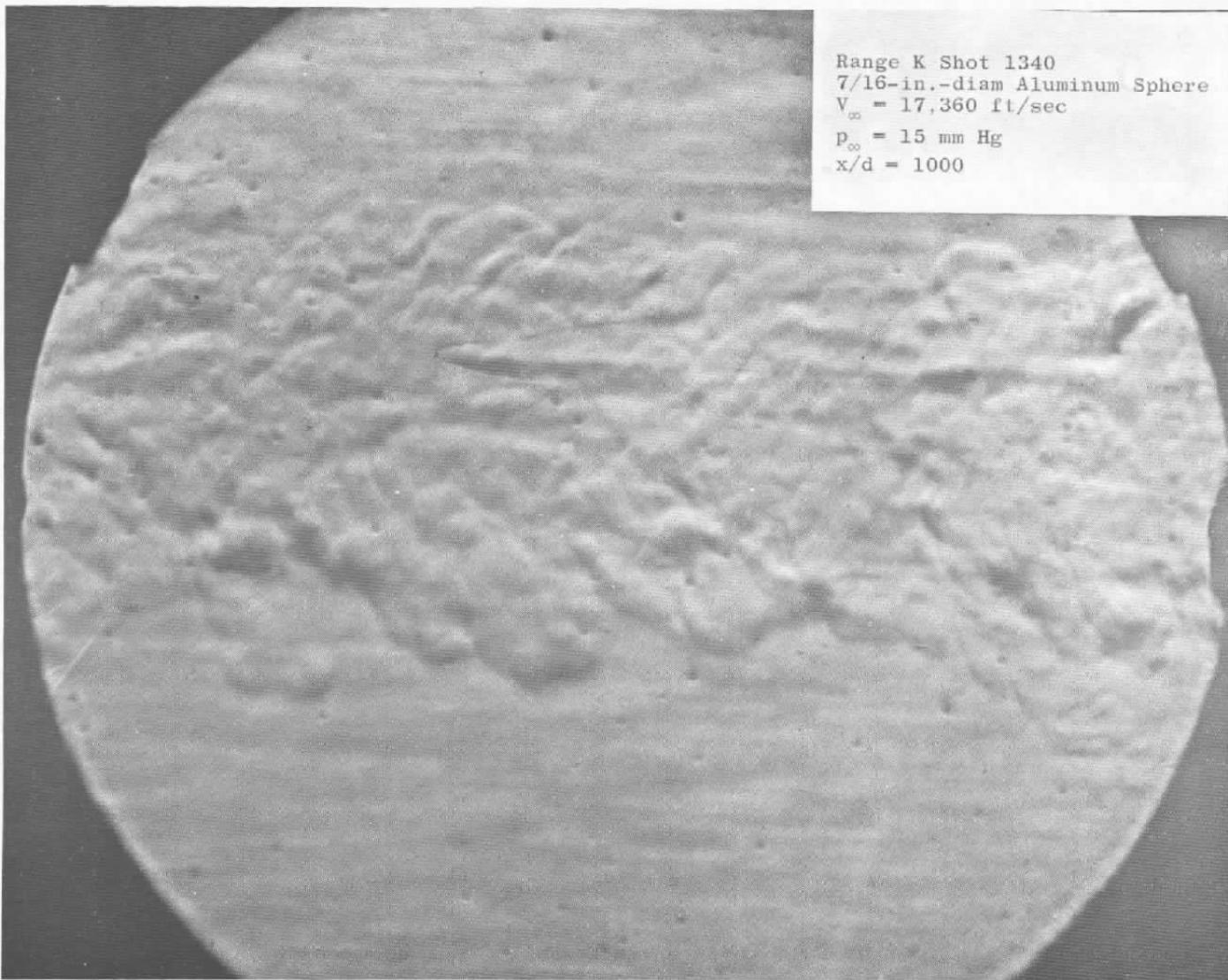
Fig. 7 Turbulent Wake behind a Sphere at an Ambient Pressure of 15 mm Hg ($V_\infty \approx 17,400$ ft/sec)

Adjustable Short

Variable Attenuator

Detector

40-db Amplifier

Power Supply

Klystron 35 kmc

Ferrite Isolator

Hybrid Tee

Oscilloscope

45-deg Bend

Bulkhead Flange

Tank Wall

Horn Lens
$\emptyset$ = 6 in.
f = 22 in.
d = 2 in. at -10 db

$\mathcal{C}$ of Range Tank

f

Microwave Absorber
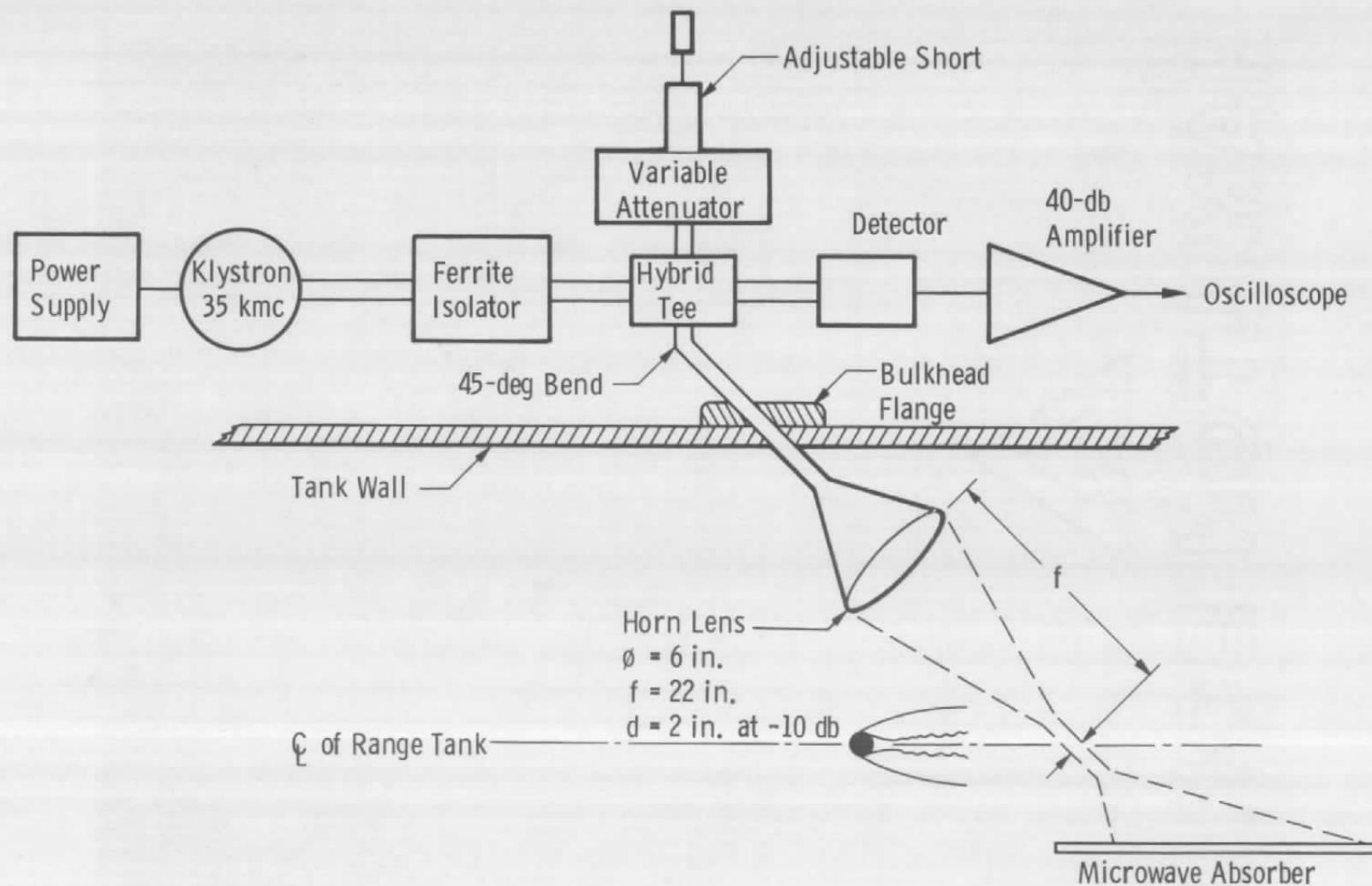
Fig. 8  Oblique Doppler Radar Results (35-kmc)

Range K Shot 1180
1/8-in.-diam Sphere
$V_\infty$ = 11,500 ft/sec
$p_\infty$ = 300 mm Hg
x/d = 14,100
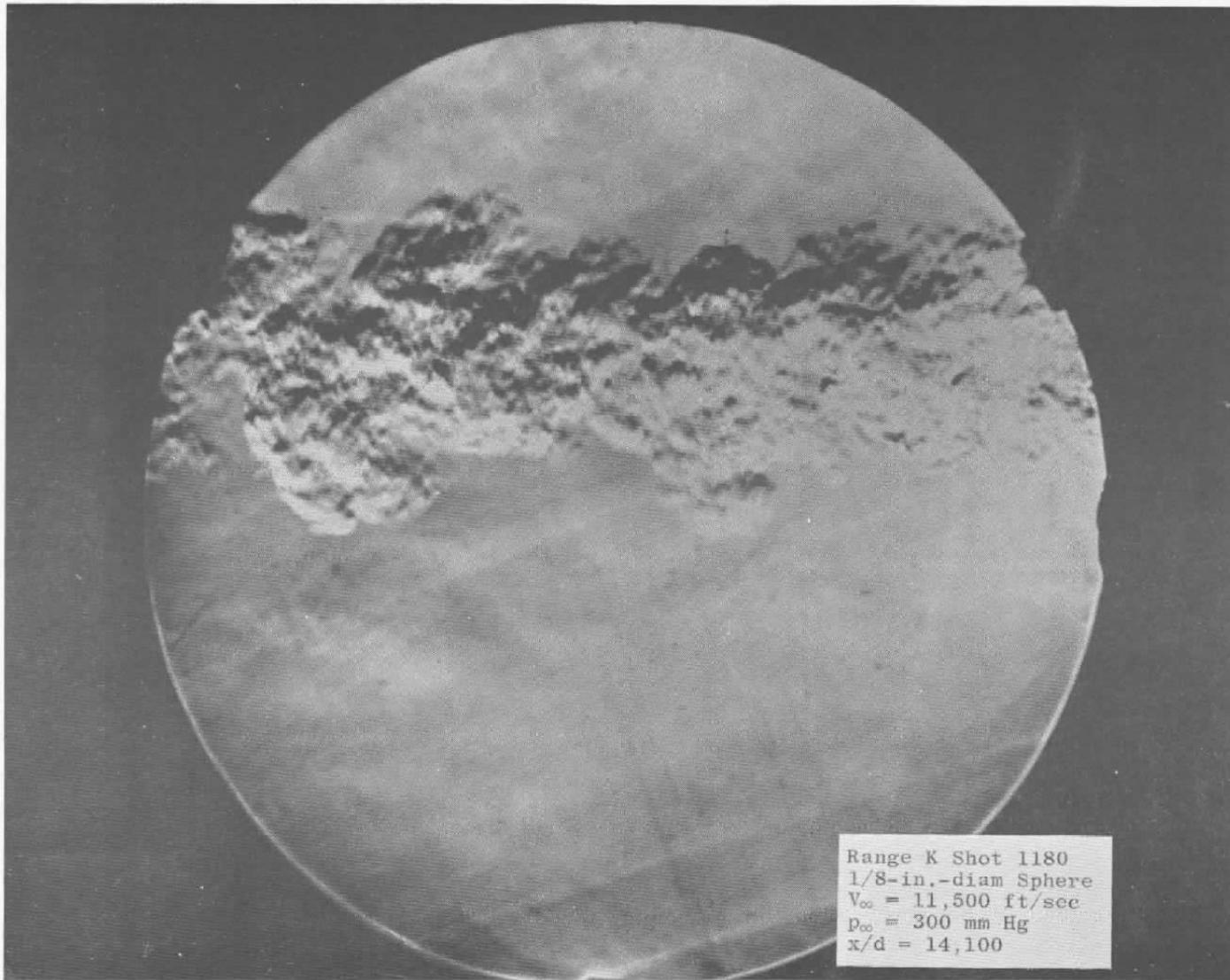
Fig. 9  Turbulent Far Wake for a Sphere
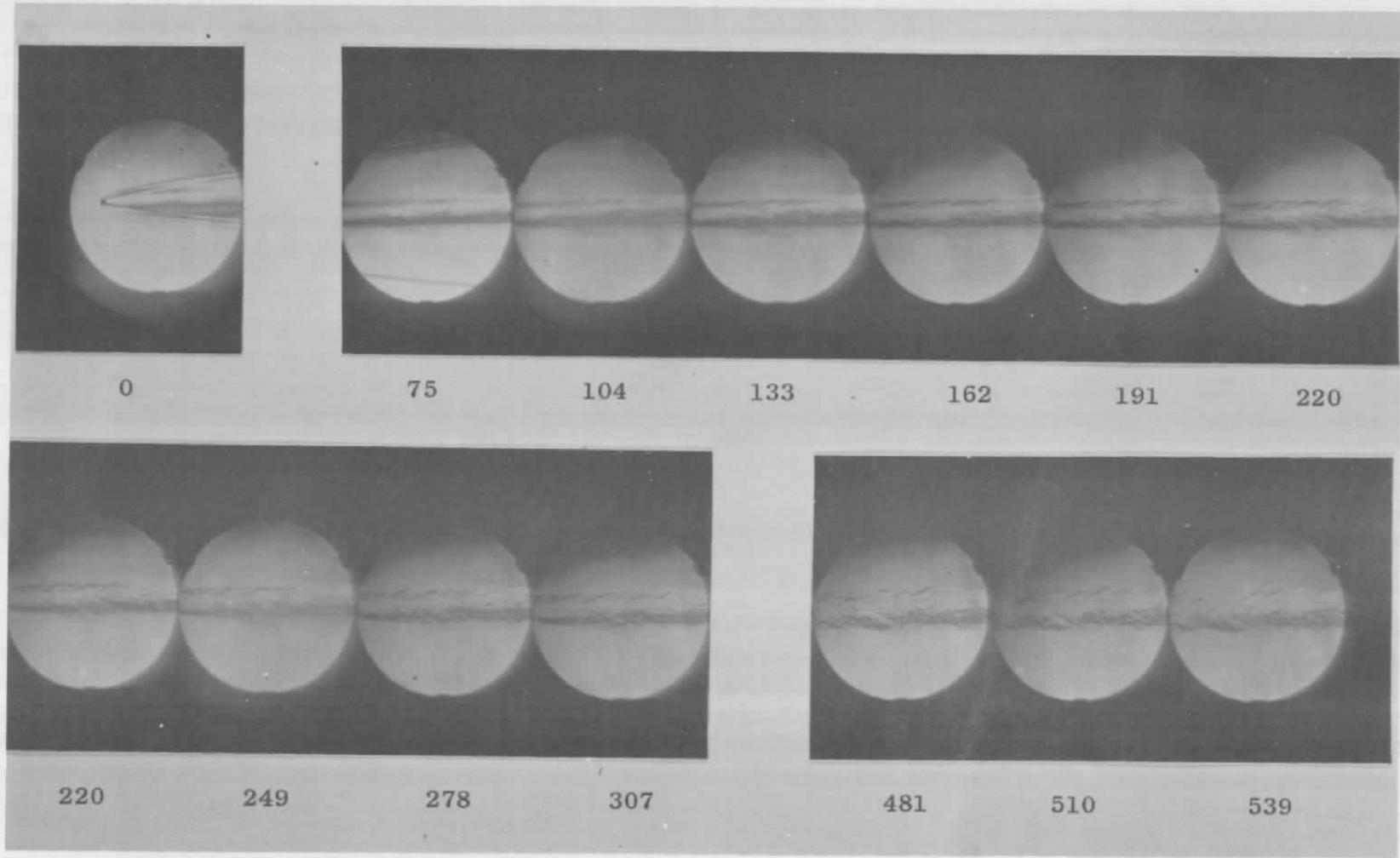
Fig. 10  Turbulent Wake behind a Sphere at an Ambient Pressure of 100 mm Hg at a Velocity of 10,900 ft/sec

11      34      108      174

340      1900      14,100      18,000
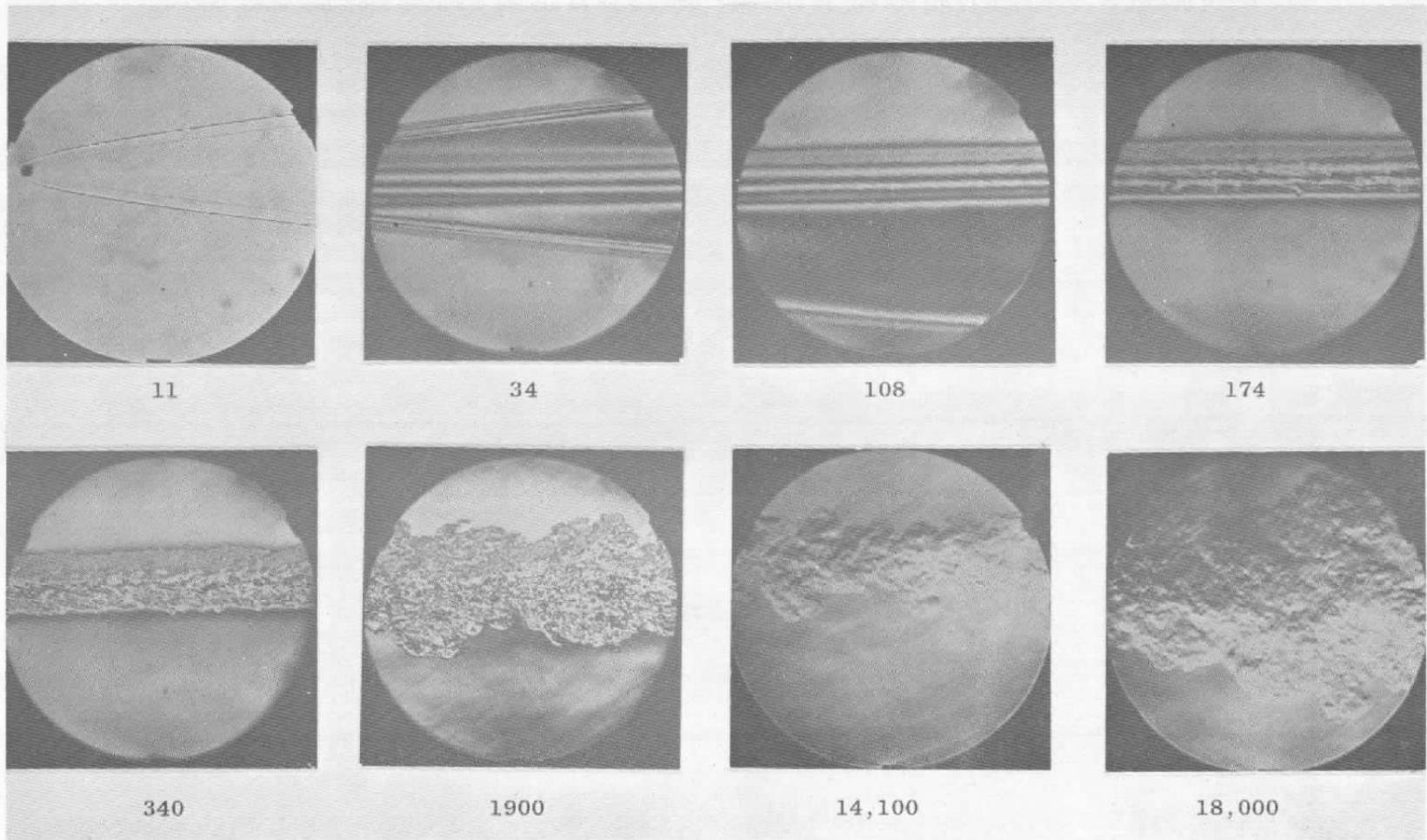
Fig. 11 Turbulent Wake behind a Sphere at an Ambient Pressure of 300 mm Hg (11,500 $\leq V_\infty \leq$ 13,500 ft/sec)
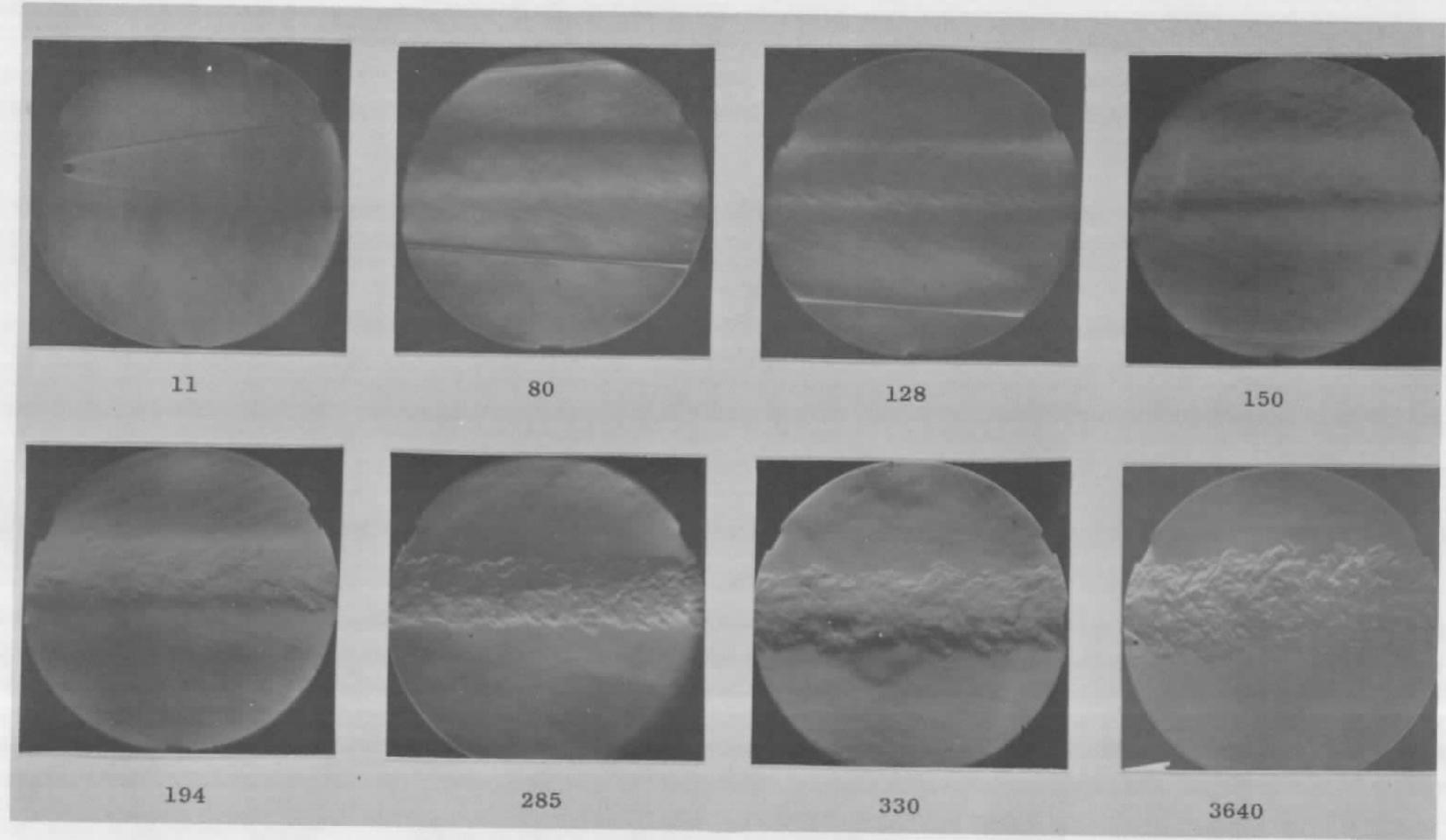
Fig. 12  Turbulent Wake behind a Sphere at an Ambient Pressure of 35 mm Hg ($19,000 \leq V_\infty \leq 21,000$)
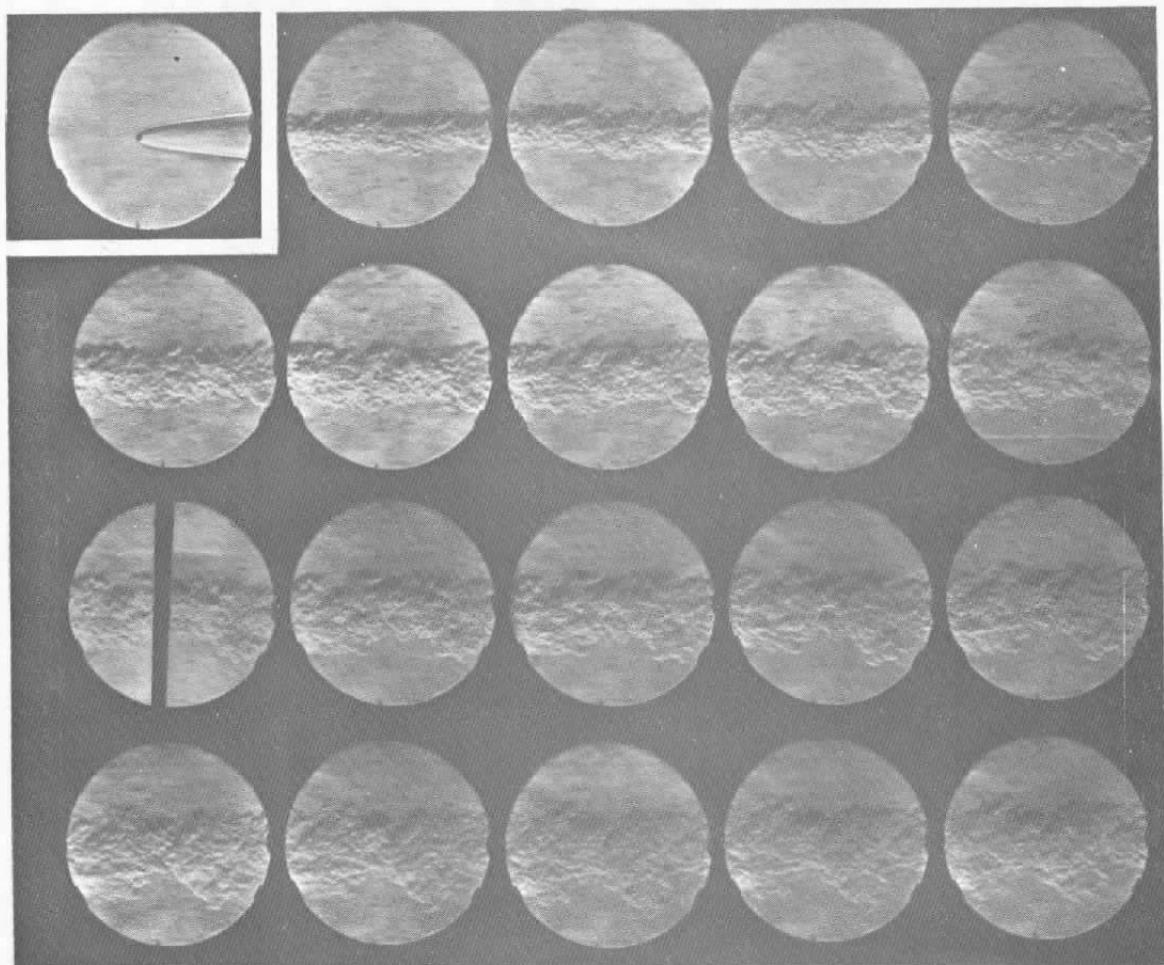
Range K Shot 1372
1/4-in.-diam Nylon Sphere
Frame Spacing is 470
 Body Diameters

Fig. 13 Turbulent Far Wake of a Sphere at 20,650 ft/sec and an Ambient Pressure of 50 mm Hg
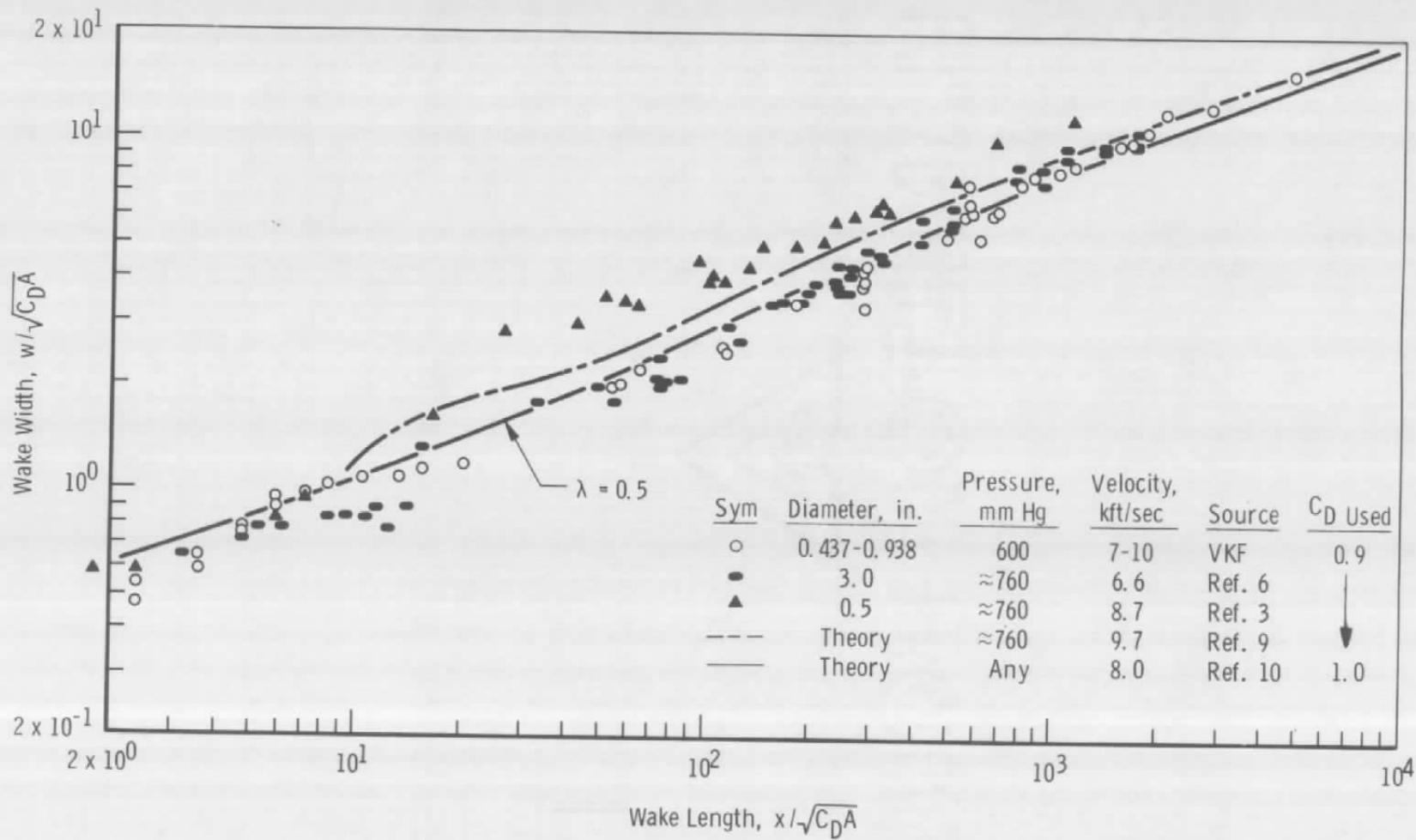
Fig. 14 The Growth of the Inner Turbulent Wake behind a Sphere ( $7000 \leq V_\infty \leq 10,000$ ft/sec )
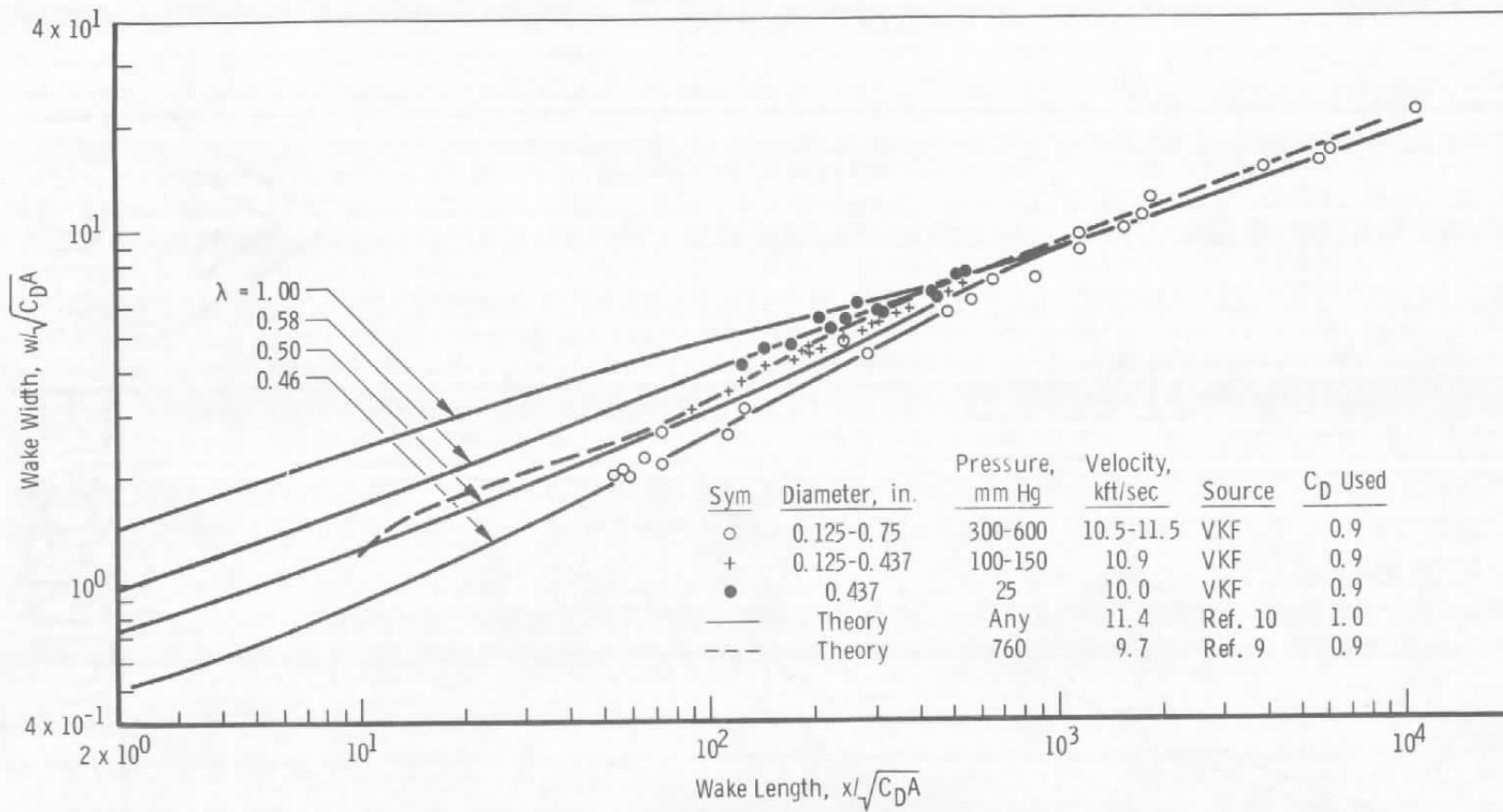
Fig. 15 The Growth of the Inner Turbulent Wake behind a Sphere (10,000 ≤ V∞ ≤ 11,500 ft/sec)
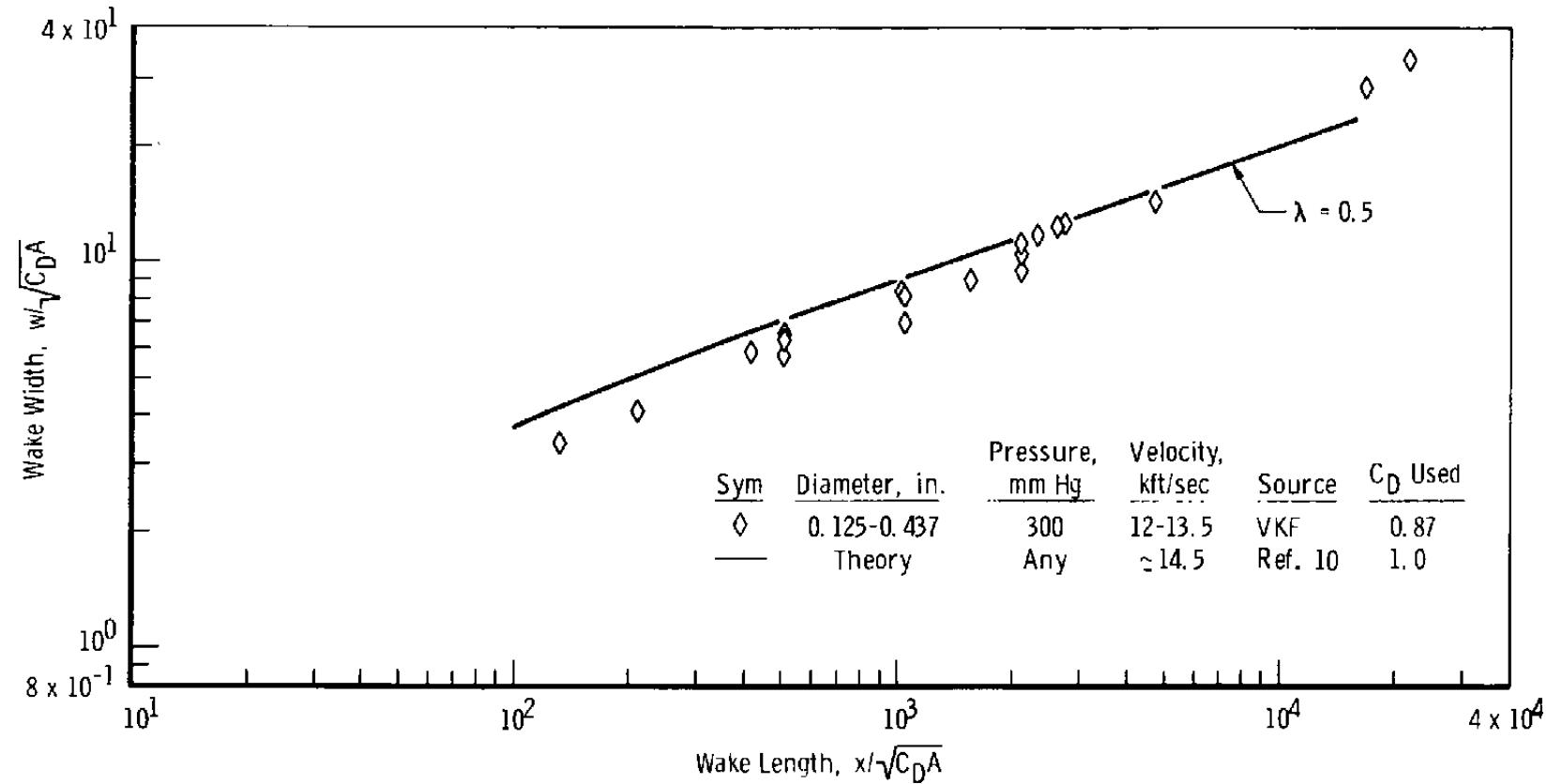
Fig. 16 The Growth of the Inner Turbulent Wake behind a Sphere (12,000 $\leq V_\infty \leq$ 13,500 ft/sec)
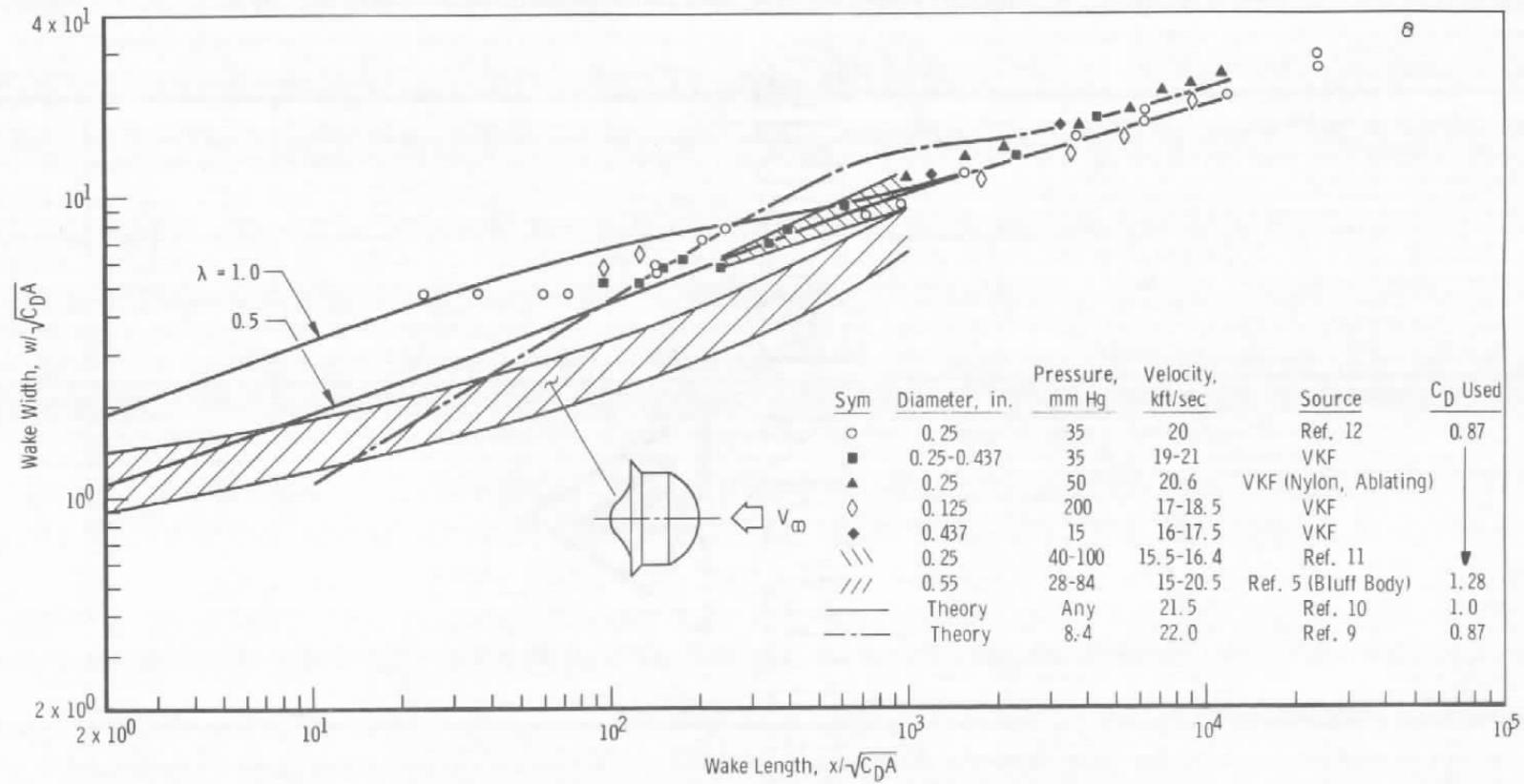
Fig. 17  The Growth of the Inner Turbulent Wake behind a Sphere ($15{,}000 \leq V_\infty \leq 21{,}000$ ft/sec)

| Sym | Velocity, kft/sec | Source | $C_D$ Used |
|-----|-------------------|--------|------------|
| ○ | 20 | Ref. 12 | 0.87 |
| ● | 7-11.5 | VKF | 0.90 |
| ★ | 12-13.5 | VKF | 0.87 |
| ▲ | 16-21 | VKF | 0.87 |



$$w/\sqrt{C_D A} \sim (x/\sqrt{C_D A})^{1/3}$$

Wake Width, $w/\sqrt{C_D A}$

Wake Length, $x/\sqrt{C_D A}$
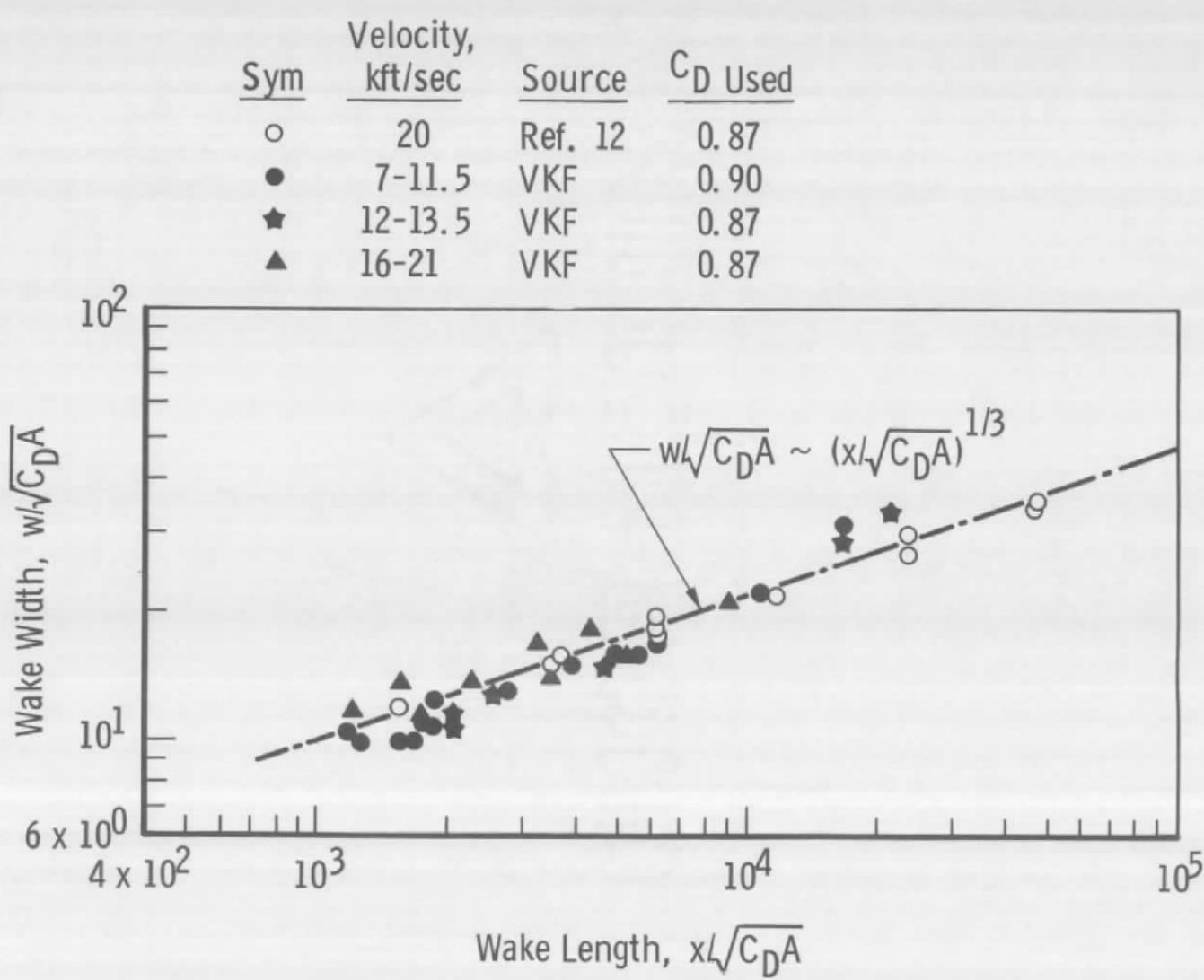
Fig. 18  The Growth of the Turbulent Far Wake

| | Model Type | Semivertex Angle, deg | $(Re/in.)_\infty \times 10^{-5}$ | $(x/d)_{tr}$ | Source |
|---|---|---|---|---|---|
| 1 | Cone | 12.5 | 0.07-2.2 | 0.7-1.6 | Ref. 14 |
| 2 | Sphere | | 0.42-3.2 | 1.4-2.7 | |
| 3 | Cone | 12.5 | 0.4 -4.7 | 2.7-5.3 | |
| 4 | Wedge | 2.5-22.5 | 0.7 -2.4 | 3.0-10.0 | |
| 5 | Cylinder | | 0.74-2.4 | 1.6-6.3 | |
| 6 | Sphere | | 1.2-11.5 | 2.4-7.2 | |
| 7 | Sphere | | 0.43-2.3 | 17.4-28.5 | |
| 8 | Cone | 10-15 | 2.5-27.5 | 9.9-15.0 | |
| 9 | Sphere | | 1.7- 6.9 | 7.8-15.0 | |
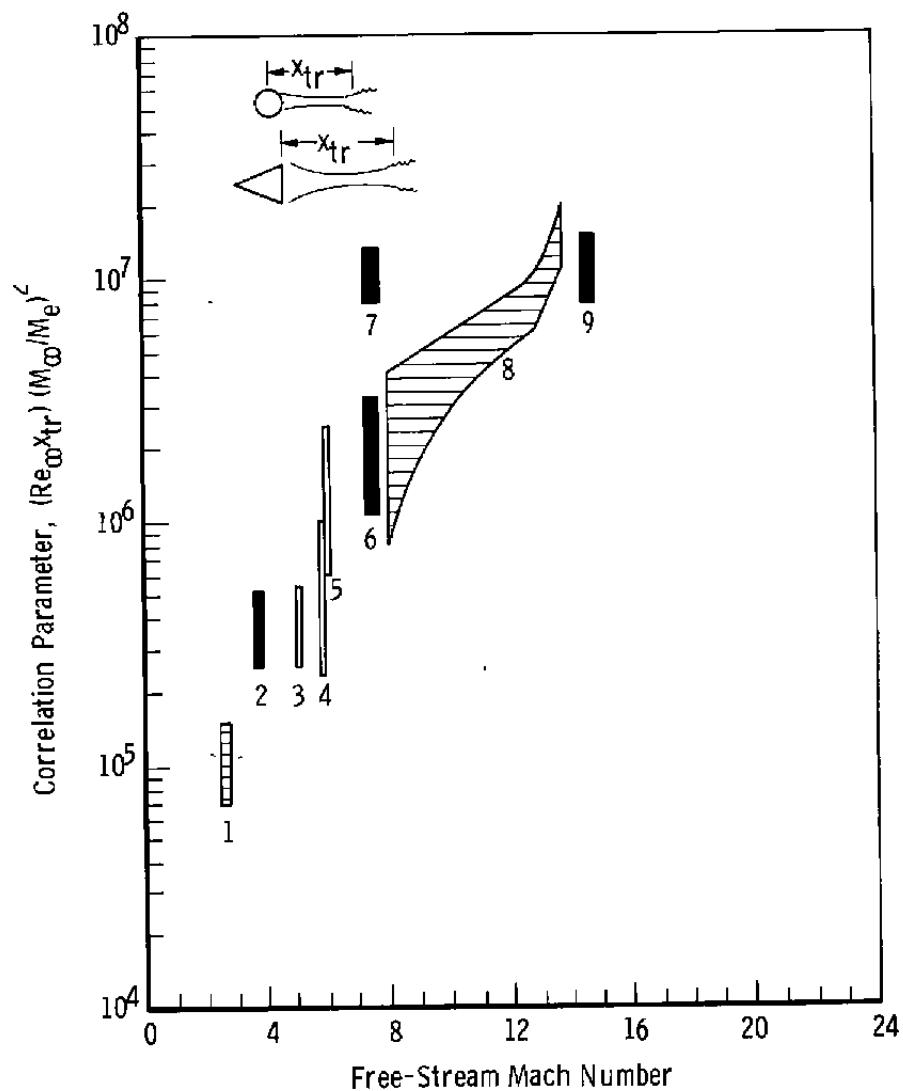


Fig. 19 Unified Wake Transition Correlation for Small Scale Models
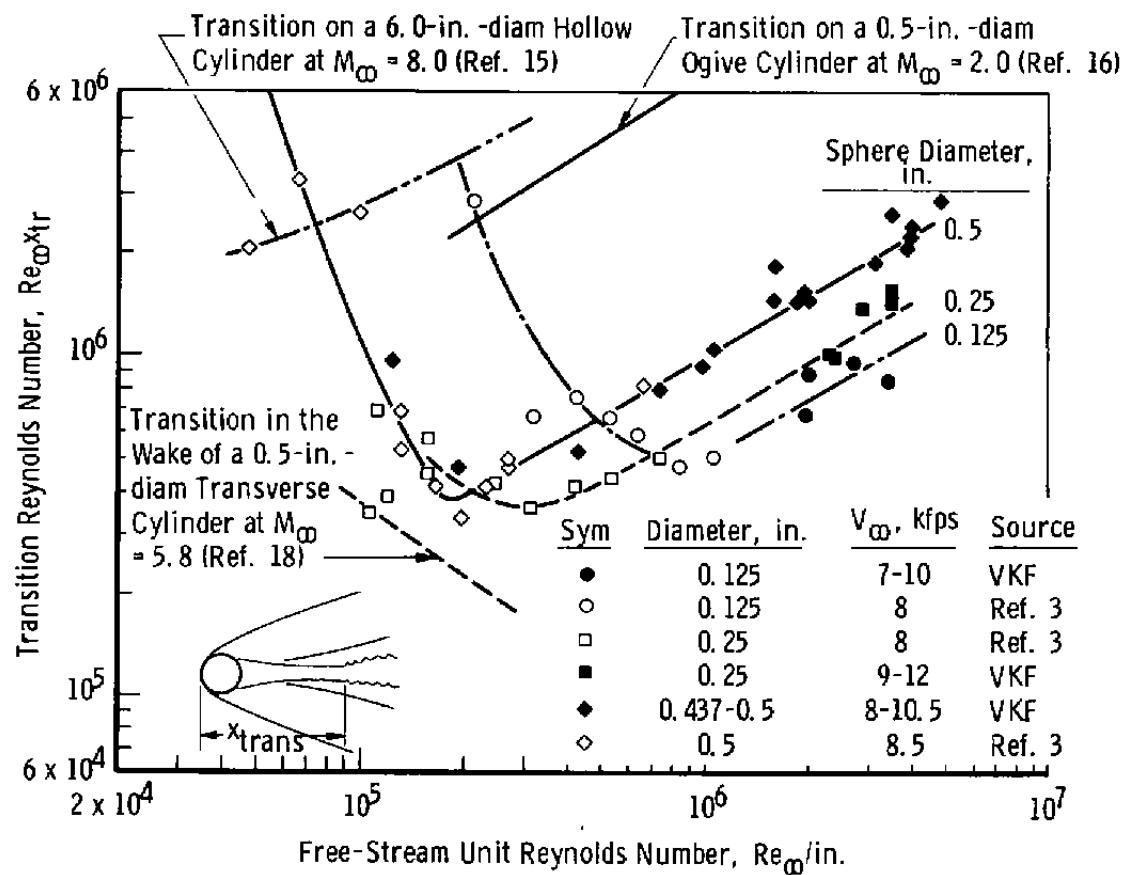
Fig. 20  Transition from Laminar to Turbulent Flow for Spheres (7000 $\leq V_\infty \leq$ 10,000 ft/sec)
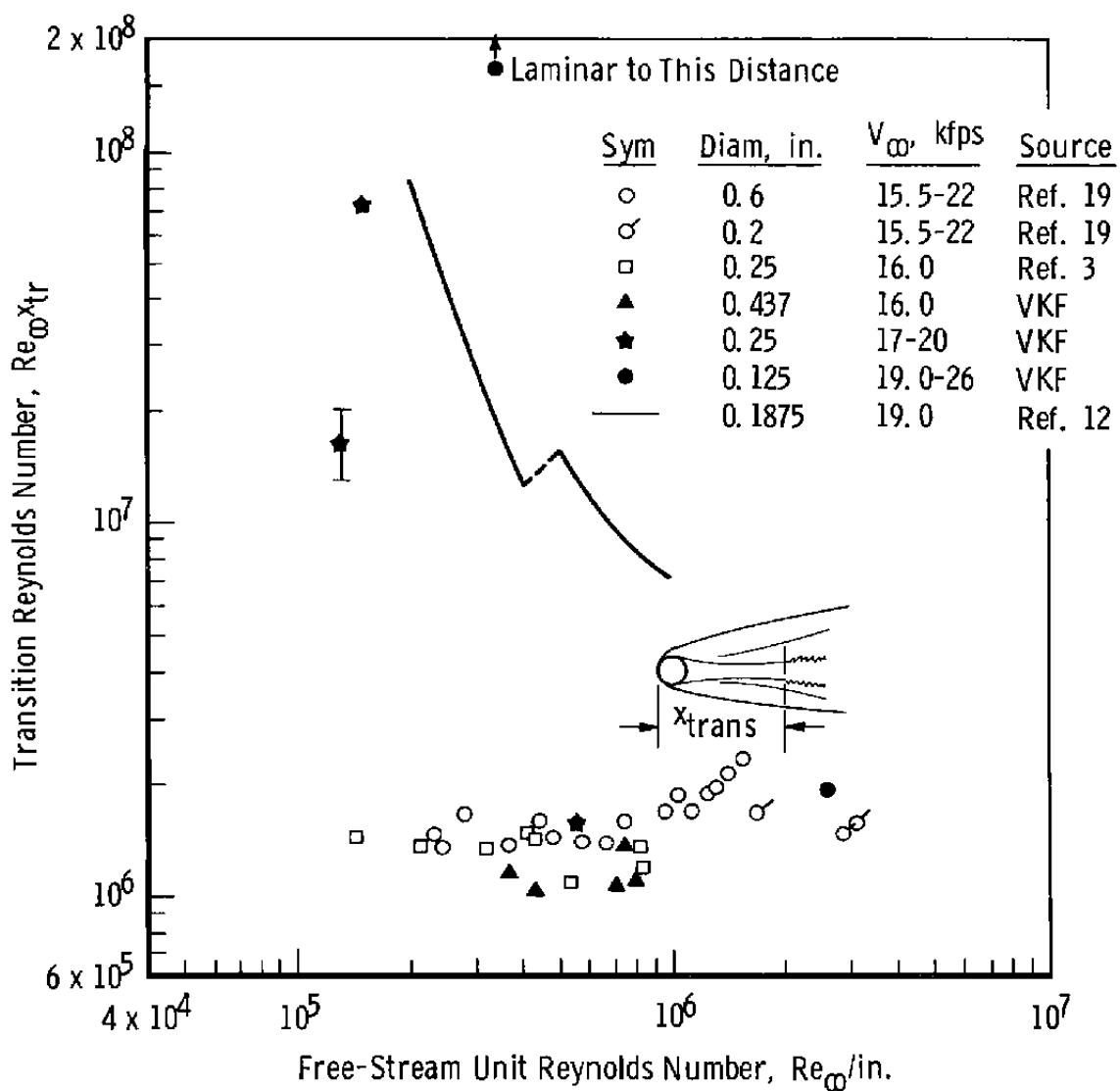
Fig. 21 Transition from Laminar to Turbulent Flow for Spheres ( 15,500 $\leq$ V$_\infty$ $\leq$ 26,000 ft/sec)
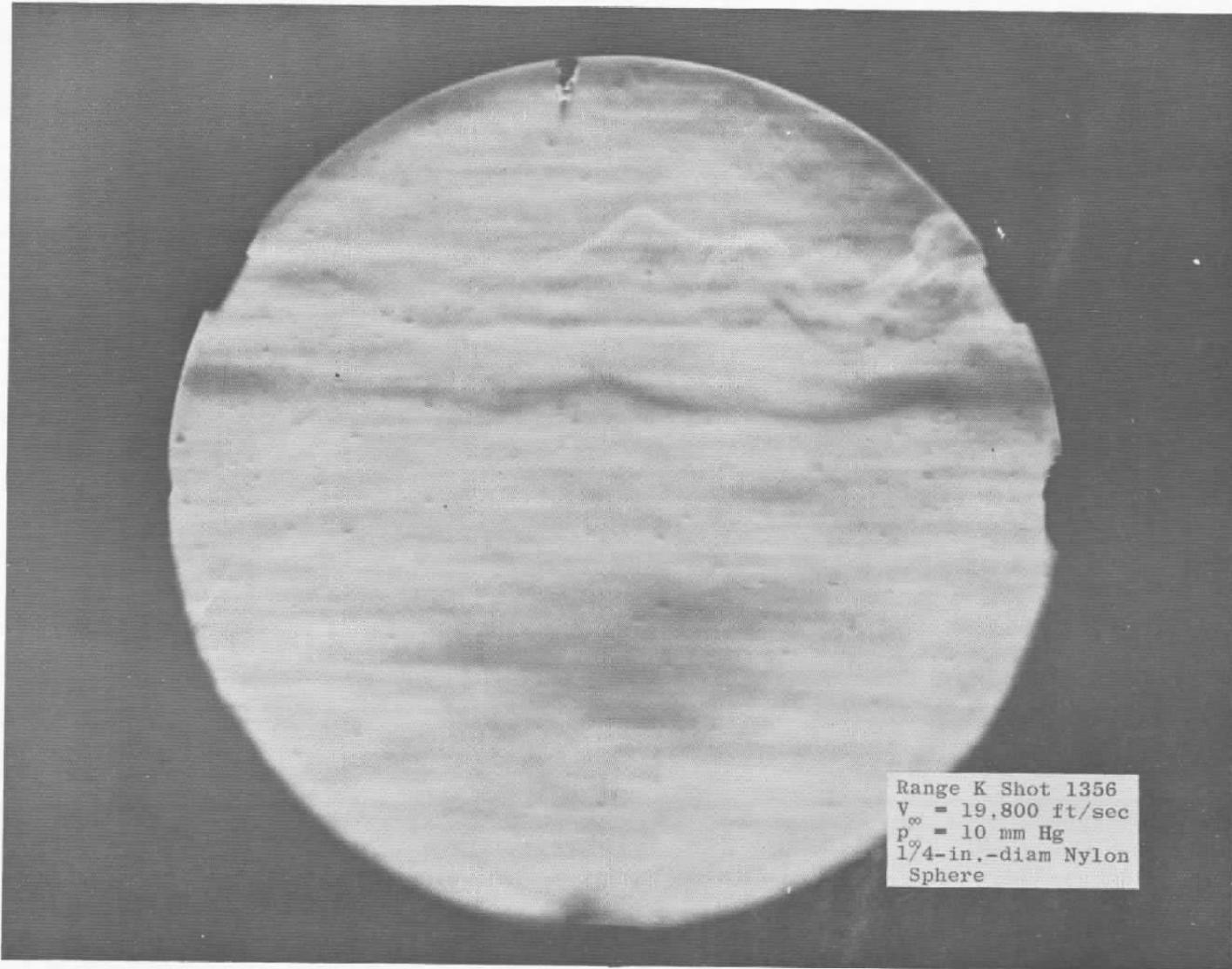
Range K Shot 1356
$V_\infty$ = 19,800 ft/sec
$p_\infty$ = 10 mm Hg
1/4-in.-diam Nylon
  Sphere

Fig. 22a  Transition in the Wake of High Speed Sphere
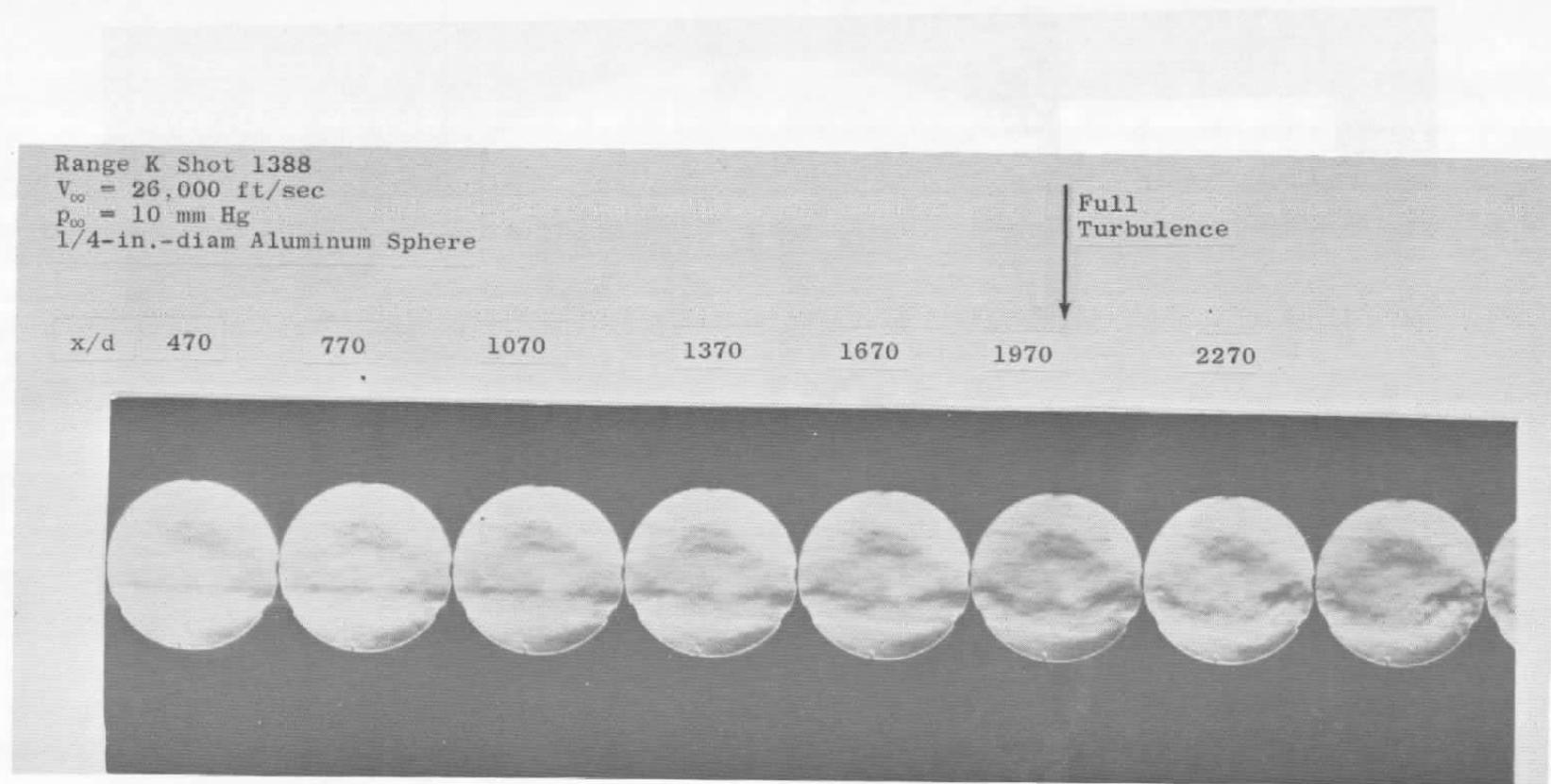
Fig. 22b  Transition in the Wake of a High Speed Sphere
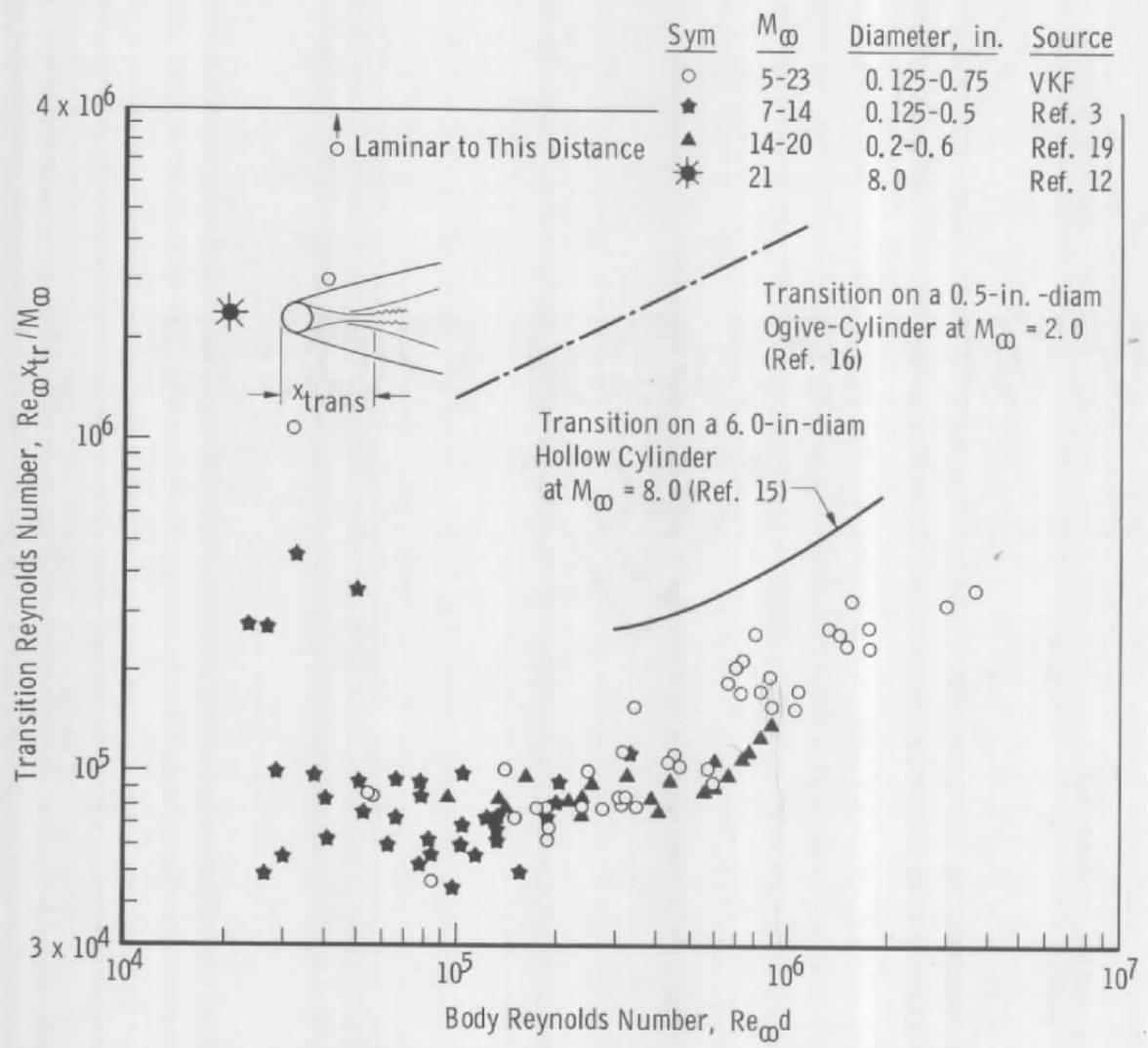
Fig. 23 Transition from Laminar to Turbulent Flow in the Wake of a Sphere
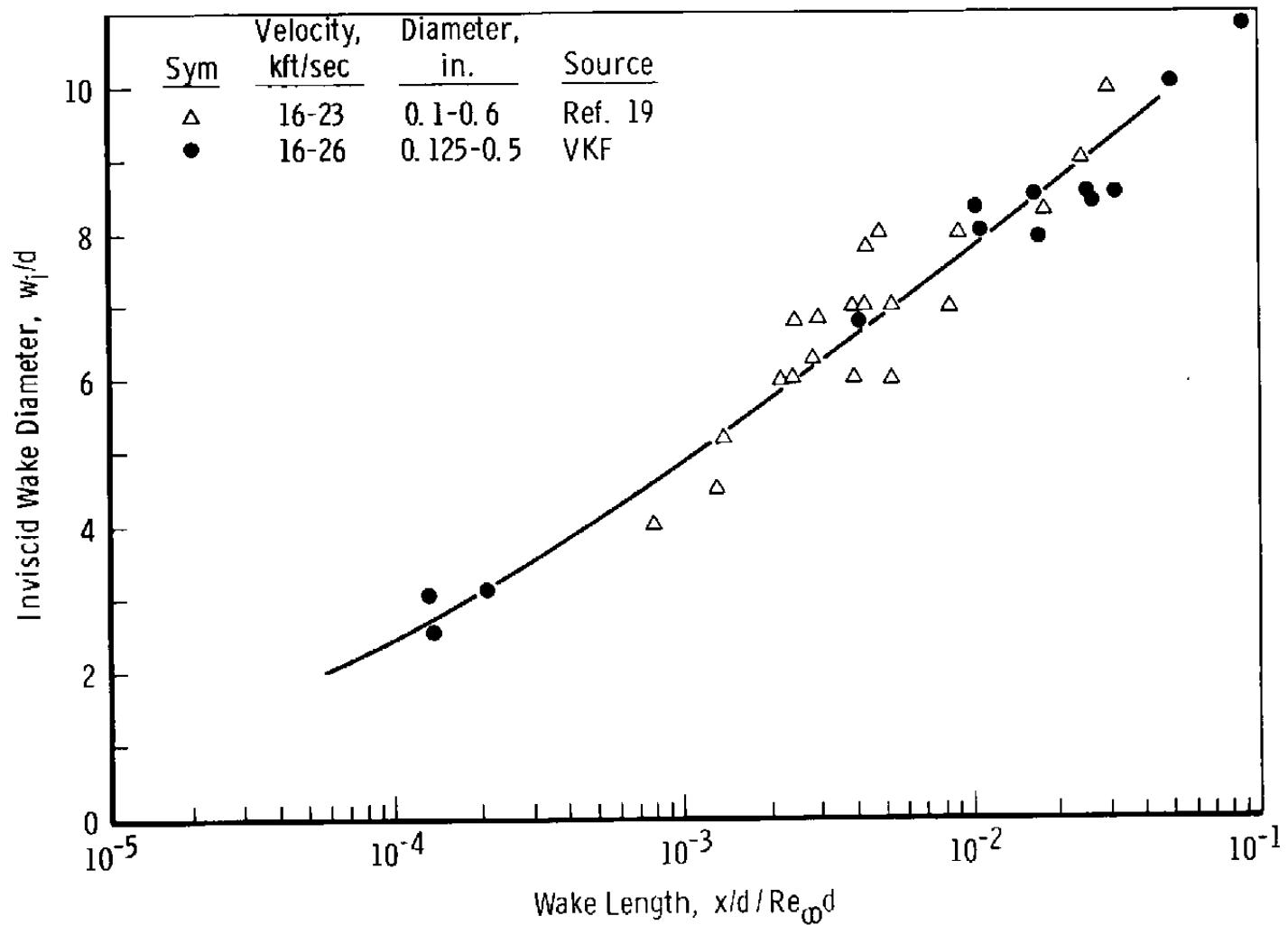
Fig. 24  Growth of the Inviscid Wake of a Sphere
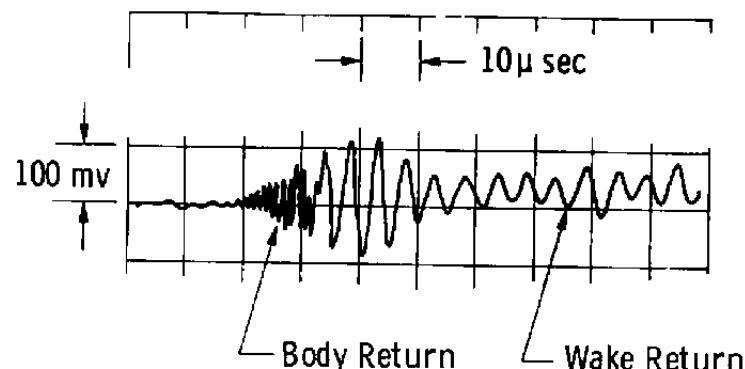
(a)

0.125-in.-diam Steel Sphere:
Pressure - 200 mm Hg
Velocity - 17,300 ft/sec
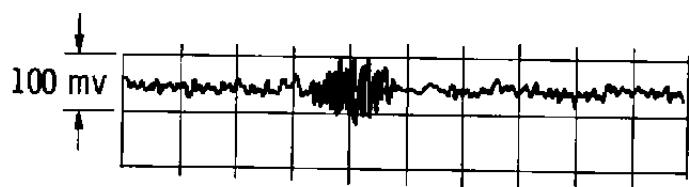
(b)

0.125-in.-diam Tungsten
Carbide Sphere:
Pressure - 200 mm Hg
Velocity - 19,500 ft/sec
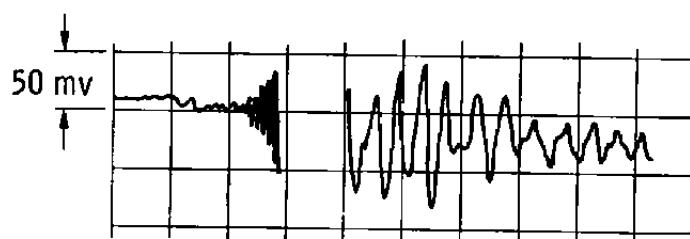
(c)

0.125-in.-diam Tungsten
Carbide Sphere:
Pressure - 730 mm Hg
Velocity - 17,100 ft/sec

Fig. 25  Results from a 35-kmc Oblique Doppler Radar System

Oblique Focused Doppler Radar

| Sym | $V_\infty$, kfps | $P_\infty$, mm Hg | Material | Diameter, in. | Source |
|---|---|---|---|---|---|
| ☆ | 15.6-21.0 | 35 | Aluminum | 0.25-0.437 | VKF |
| ★ | 17.4-18.5 | 200 | Steel | 0.125 | |
| ● | 20.5 | 50 | Nylon | 0.25 | |
| ◆ | 17.0 | 734 | Tungsten Carbide | 0.125 | |
| —··— | 17.6-19.6 | 50-100 | Copper | 0.2 -0.6 | Ref. 23 |

Schlieren

| | | | | | |
|---|---|---|---|---|---|
| △ | 10.0-11.0 | 100 | Aluminum | 0.437 | VKF |
| - - - | 7.6 | ≈760 | Aluminum | 0.50 | Ref. 3 |
| ——— | Theory | | | | Ref. 9 |

Luminosity-Drum Camera Technique

| | | | | | |
|---|---|---|---|---|---|
| —·— | 13.5-14.0 | 40-60 | Lexan | 0.55 | Ref. 22 |
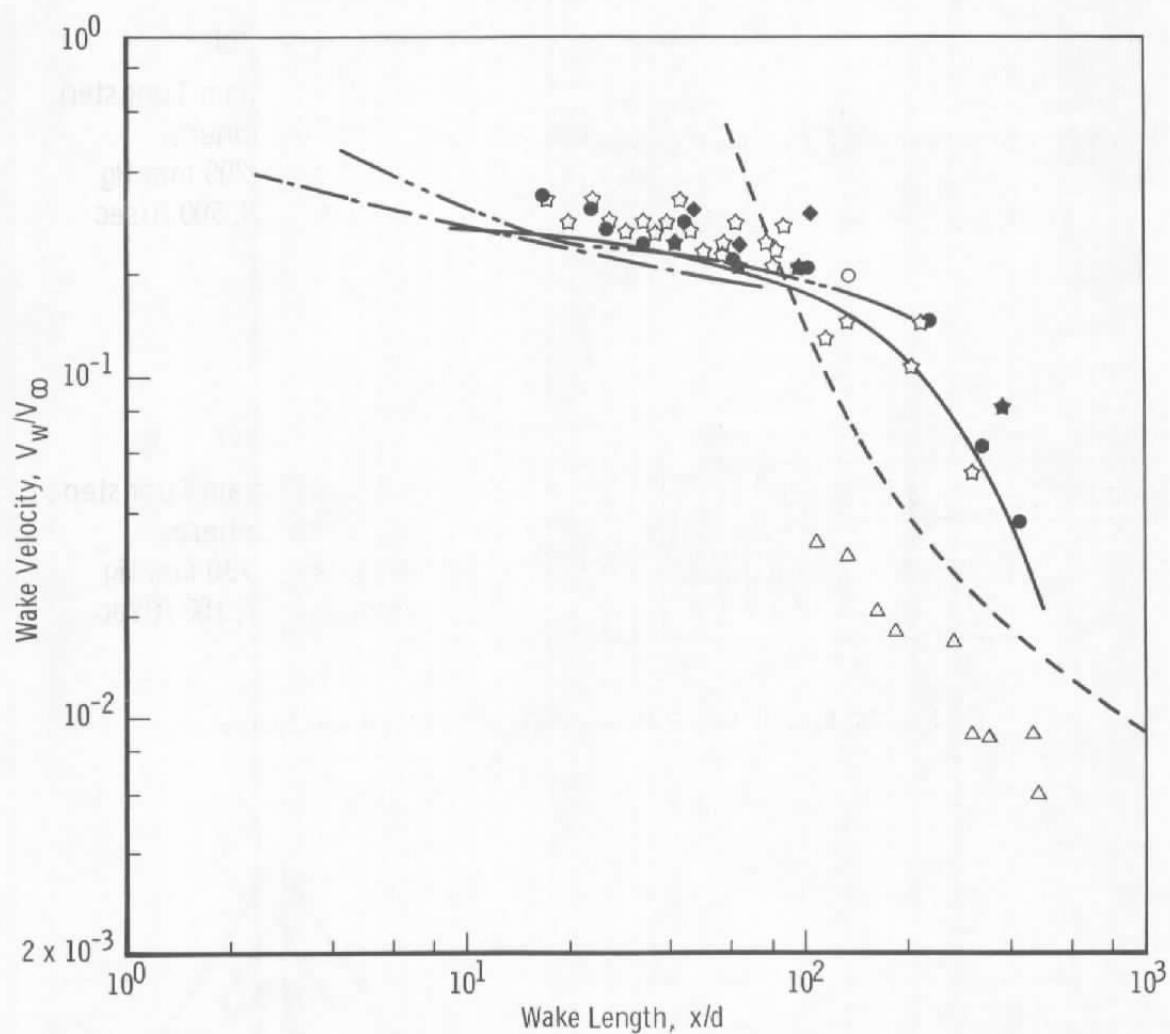


Fig. 26 Wake Velocity behind a Sphere

Fig. 27 Variation of Shock Wave Shape with Velocity of a Sphere
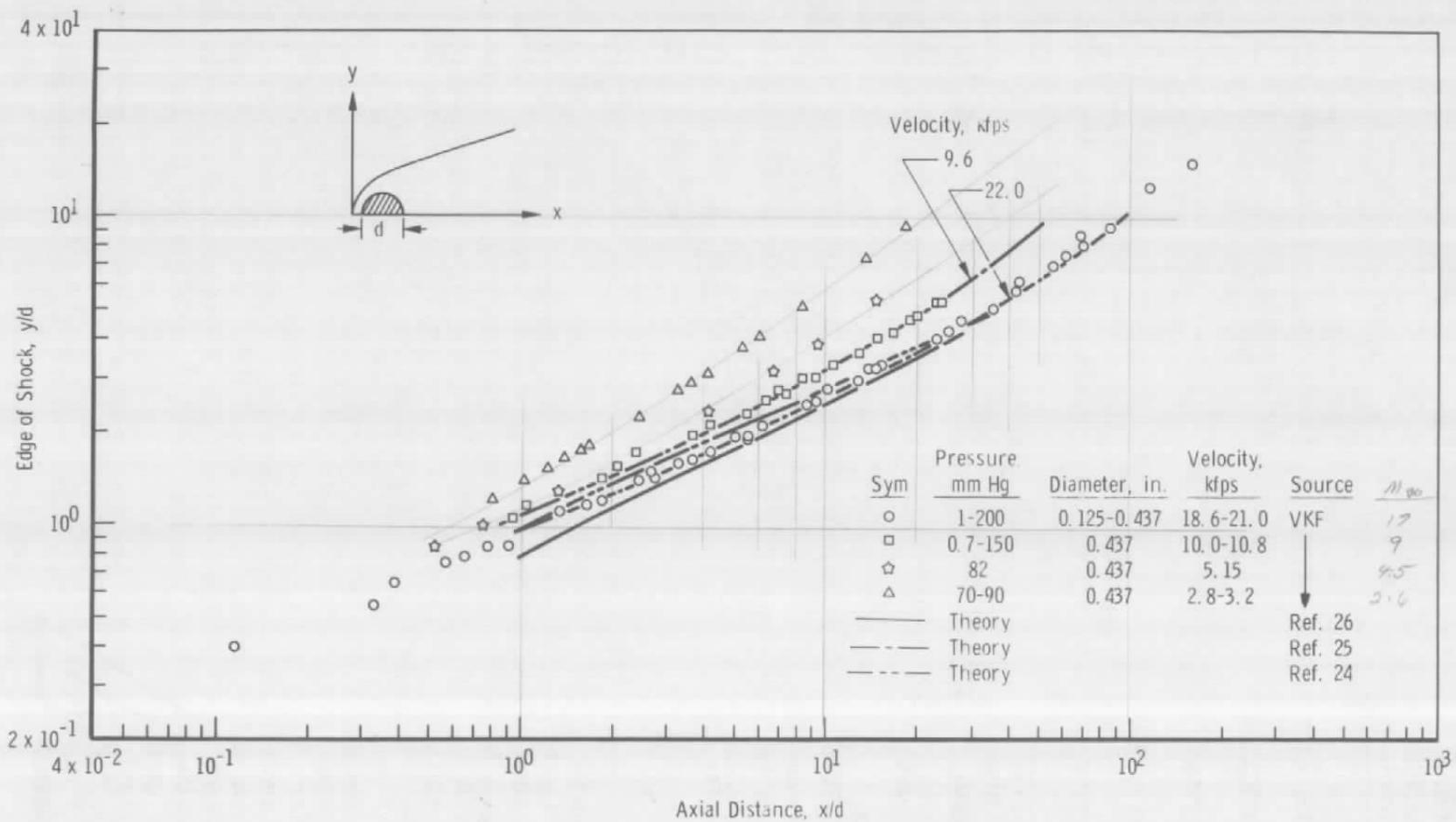
## DOCUMENT CONTROL DATA - R&D

*(Security classification of title, body of abstract and indexing annotation must be entered when the overall report is classified)*

| 1 ORIGINATING ACTIVITY (Corporate author) | 2a REPORT SECURITY CLASSIFICATION |
|---|---|
| Arnold Engineering Development Center | UNCLASSIFIED |
| ARO, Inc., Operating Contractor | 2b GROUP |
| Arnold Air Force Station, Tennessee | N/A |

**3 REPORT TITLE**

TURBULENT WAKE AND SHOCK SHAPE OF HYPERVELOCITY SPHERES (U)

**4 DESCRIPTIVE NOTES (Type of report and inclusive dates)**

N/A

**5 AUTHOR(S) (Last name, first name, initial)**

Bailey, A. B., ARO, Inc.

| 6 REPORT DATE | 7a TOTAL NO OF PAGES | 7b NO OF REFS |
|---|---|---|
| July 1966 | 54 | 26 |

| 8a CONTRACT OR GRANT NO. | 9a ORIGINATOR'S REPORT NUMBER(S) |
|---|---|
| AF40(600)-1200 | |
| b PROJECT NO ▮▮▮▮ | AEDC-TR-66-32 |
| c Program Element 65402234 | 9b OTHER REPORT NO(S) (Any other numbers that may be assigned this report) |
| d Task ▮▮▮▮▮▮ | N/A |

**10 AVAILABILITY/LIMITATION NOTICES** Qualified requesters may obtain copies of this report from DDC and transmittal to foreign governments or foreign nationals must have prior approval of AEDC.

| 11 SUPPLEMENTARY NOTES | 12 SPONSORING MILITARY ACTIVITY Arnold |
|---|---|
| N/A | Engineering Development Center (AEDC) Air Force Systems Command (AFSC) Arnold Air Force Station, Tennessee |

**13 ABSTRACT**

Experiments have been conducted to study some of the properties of the inner turbulent wake behind high speed spheres in free flight over a wide range of velocity and pressure. Schlieren and shadowgraph techniques have been used to photograph the wake. It has been shown that the growth of the inner wake close to the body is a function of velocity and ambient pressure. In the very far wake (x/d ≳ 1000) it has been shown experimentally that wake growth follows a 1/3 power law independent of velocity and ambient pressure. Experimental measurements of the location of transition from laminar to turbulent flow in the inner viscous wake have been shown to be dependent upon unit Reynolds number. Approximate axial velocity distributions in the inner viscous wake have been measured with oblique doppler radar techniques and a schlieren drum camera system. These two systems measure such widely different velocities that it has been concluded that they measure the velocity at different radial positions in a wake which has strong radial gradients in velocity. Finally, a study of the shock shape for spheres for a wide range of pressure and velocity has shown that the shape is dependent upon Mach number rather than velocity and is independent of ambient pressure. This comment does not apply to the standoff distance. (U)

**DD** FORM 1 JAN 64 **1473**

| 14 KEY WORDS | LINK A | | LINK B | | LINK C | |
|---|---|---|---|---|---|---|
| | ROLE | WT | ROLE | WT | ROLE | WT |
| wake velocity | | | | | | |
| wake transition | | | | | | |
| shock shape | | | | | | |
| turbulent wake | | | | | | |
| inviscid wake | | | | | | |

## INSTRUCTIONS

1. ORIGINATING ACTIVITY: Enter the name and address of the contractor, subcontractor, grantee, Department of Defense activity or other organization (corporate author) issuing the report.

2a. REPORT SECURITY CLASSIFICATION: Enter the overall security classification of the report. Indicate whether "Restricted Data" is included. Marking is to be in accordance with appropriate security regulations.

2b. GROUP: Automatic downgrading is specified in DoD Directive 5200.10 and Armed Forces Industrial Manual. Enter the group number. Also, when applicable, show that optional markings have been used for Group 3 and Group 4 as authorized.

3. REPORT TITLE: Enter the complete report title in all capital letters. Titles in all cases should be unclassified. If a meaningful title cannot be selected without classification, show title classification in all capitals in parenthesis immediately following the title.

4. DESCRIPTIVE NOTES: If appropriate, enter the type of report, e.g., interim, progress, summary, annual, or final. Give the inclusive dates when a specific reporting period is covered.

5. AUTHOR(S): Enter the name(s) of author(s) as shown on or in the report. Enter last name, first name, middle initial. If military, show rank and branch of service. The name of the principal author is an absolute minimum requirement.

6. REPORT DATE: Enter the date of the report as day, month, year, or month, year. If more than one date appears on the report, use date of publication.

7a. TOTAL NUMBER OF PAGES: The total page count should follow normal pagination procedures, i.e., enter the number of pages containing information.

7b. NUMBER OF REFERENCES: Enter the total number of references cited in the report.

8a. CONTRACT OR GRANT NUMBER: If appropriate, enter the applicable number of the contract or grant under which the report was written.

8b, 8c, & 8d. PROJECT NUMBER: Enter the appropriate military department identification, such as project number, subproject number, system numbers, task number, etc.

9a. ORIGINATOR'S REPORT NUMBER(S): Enter the official report number by which the document will be identified and controlled by the originating activity. This number must be unique to this report.

9b. OTHER REPORT NUMBER(S): If the report has been assigned any other report numbers (either by the originator or by the sponsor), also enter this number(s).

10. AVAILABILITY/LIMITATION NOTICES: Enter any limitations on further dissemination of the report, other than those imposed by security classification, using standard statements such as:

(1) "Qualified requesters may obtain copies of this report from DDC."

(2) "Foreign announcement and dissemination of this report by DDC is not authorized."

(3) "U. S. Government agencies may obtain copies of this report directly from DDC. Other qualified DDC users shall request through

_____ ."

(4) "U. S. military agencies may obtain copies of this report directly from DDC. Other qualified users shall request through

_____ ."

(5) "All distribution of this report is controlled. Qualified DDC users shall request through

_____ ."

If the report has been furnished to the Office of Technical Services, Department of Commerce, for sale to the public, indicate this fact and enter the price, if known.

11. SUPPLEMENTARY NOTES: Use for additional explanatory notes.

12. SPONSORING MILITARY ACTIVITY: Enter the name of the departmental project office or laboratory sponsoring (paying for) the research and development. Include address.

13. ABSTRACT: Enter an abstract giving a brief and factual summary of the document indicative of the report, even though it may also appear elsewhere in the body of the technical report. If additional space is required, a continuation sheet shall be attached.

It is highly desirable that the abstract of classified reports be unclassified. Each paragraph of the abstract shall end with an indication of the military security classification of the information in the paragraph, represented as (TS), (S), (C), or (U).

There is no limitation on the length of the abstract. However, the suggested length is from 150 to 225 words.

14. KEY WORDS: Key words are technically meaningful terms or short phrases that characterize a report and may be used as index entries for cataloging the report. Key words must be selected so that no security classification is required. Identifiers, such as equipment model designation, trade name, military project code name, geographic location, may be used as key words but will be followed by an indication of technical context. The assignment of links, rules, and weights is optional.